Chapter 5
Phase Diagrams with the CALPHAD Method

5.1 Introduction

Materials science investigates the structure, properties, preparation and processing of materials. These investigations are increasingly supported by models based on concepts of chemistry, physics and crystallography as modern society is constantly looking for new and innovative materials to enable and support new technologies.

If one considers that 86 of the about 100 elements known to man (excluding the inert gasses and transuranic elements) combine to as many as $7.7x10^{25}$ systems (binary, ternary, quaternary up to the 86-element system), it is not surprising that as computational power became available and was developed, many modelling methods have been adopted to predict phase diagrams, material structures, material properties and processing conditions by computational methods.

One of these methods, based on the 19th century work of Gibbs, is the CALPHAD (CALculation of PHAse Diagrams) method, a completely general, extendable and theoretically meaningful technique. With this technique, experimental data is used to derive the Gibbs energy of an element or phase as a function of temperature, pressure and composition. From the Gibbs energies, the thermodynamic properties of a system can be derived and the equilibrium phase diagram can be predicted, since a phase diagram is a graphical representation of the loci of thermodynamic variables when equilibrium (lowest energy state) among the phases of a system is established under a given set of conditions [1996Pel].

A brief overview of the development of computational methods is given, as well as the software available. However, as the Thermo-Calc [1985Sun] software was used in this study, most of the emphasis will be placed on it.

5.2 History

Gibbs's famous study in 1876 provided the theoretical background for the thermodynamic examination of complex, chemically reacting systems. In 1908, Van Laar applied the Gibbs energy concepts to phase equilibria. Then, in the 1930s, Hume-Rothery [1934Hum] developed an alternative approach based on band-structures. When it became evident that his concepts could not be applied to industrially-relevant materials such as steels, nickel-based alloys and the emerging titanium and uranium alloys, interest focused on the thermodynamic approach again, especially those of Meijering and Hillert in Europe and Kaufman in America. Meijering [1957Mei] calculated a phase diagram for Ni-Cr-Cu, giving a quantitative description to all topological features of the phase diagram. This was pioneering work, as the mere interpolation of the binary systems would have yielded an erroneous diagram. Meijering had to extrapolate a lattice stability value (the relative Gibbs energy for a crystal structure of the pure element) for fcc Cr as this could not be obtained directly from experiment - it is interesting to note that these early results from Meijering have only been marginally improved over the years!

The thermodynamic approach showed that the lattice stabilities were not only related to the solubility limits, electron concentrations (or electron per atom ratios) and electrochemical (valence) factors from Hume-Rothery's band-structure theory, but that they also depend on the properties and interaction of the co-existing phases as well as on the temperature. Kaufman and Hume-Rothery had extensive discussions to try and clarify the conflict in different value sets of lattice stabilities. Not only was there the Hume-Rothery approach, with Jones and Mott [1936Mot] taking the electron per atom ratio model further, but also Engel [1949Eng] and Brewer [1963Bre] developed a method which correlates the structure of metals with the number of s and p valence electrons in the system. Their proposed lattice stabilities, based on spectroscopic data, differed as much as an order of magnitude in some cases with experimental values. In the next development, lattice stabilities were also obtained from electron energy calculations. The lack of agreement in these fundamental values delayed the more general acceptance of the CALPHAD technique. Pettifor [1972Pet], by following a Jones-type analysis, related band-structure to the density-of-state (DOS) in transition metals. These density functional calculations have confirmed the existence of wave mechanical oscillatory energy difference functions between lattices in a crystal, which is difficult to handle in an extrapolation technique like CALPHAD. Another factor that contributes to the discrepancies in theory and CALPHAD lattice stability values is that in the CALPHAD technique, positive melting temperatures are assigned to the metastable phases, while they are theoretically predicted to be mechanically unstable at absolute zero.

At the same time, two other modelling methods were developed to predict alloy properties. Already in 1949, Kikuchi [1951Kik] introduced the cluster variation model (CVM), but further development only started in the 1970s as the method requires substantial computing power. CVM is based on the mutual interactions of all the atoms, which are described in sets of clusters. The tetrahedron is the smallest cluster in a three-dimensional lattice and can thus reflect a great variety of atomic interactions. CVM is very powerful in treating order/disorder phenomena. Miedema [1988deB] developed a semi-empirical technique to predict the enthalpy of formation and interaction parameters for binary and some ternary alloys.

Despite the differences that existed, Larry Kaufman went ahead with his vision in 1970 and used the name 'CALPHAD' for a technique where one may calculate an improved phase diagram after assessing the thermodynamic properties of all the phases that may form from a set of components (elements, ions, compounds). This method is based on the axiom that complete Gibbs energy versus composition curves can be constructed for all the structures exhibited by the elements right across the complete alloy system. This involves the extrapolation of G/x (where x is the composition) curves for many phases into regions where they are metastable or unstable. The relative Gibbs energy for various crystal structures of the pure elements (lattice stabilities) in the system must, therefore, be established. Kaufman drafted a bilateral agreement to generate official meetings between the American and French experts, and he extended this invitation to representatives from the UK, Sweden and Germany. This was the birth of the CALPHAD meetings. The objectives defined by Kaufman and Ansara in 1973 are today still the CALPHAD objectives:
We believe that substantial progress can be made in a short period of time if we would arrange to work together for one week at one of our facilities to define problems, disband, carry out some individual activities, and meet again for a week at a second facility to compare results and chart future activities. (2003: www.calphad.org)

In 1977, the first CALPHAD – Computer Coupling of Phase Diagrams and Thermochemistry journal was published. Since 2000, the journal also accepts *ab initio* contributions.

5.3 Current Status

The CALPHAD technique has clearly come of age and it now allows for the calculation of complex phase equilibria equations. A number of commercial software packages are available. These include Thermo-Calc, FactSage, MTDATA, PANDAT, MALT and Exterm. An edition of the Calphad journal was dedicated to detailed overviews of these commercial packages (CALPHAD, Vol. 26, No. 2, 2002). Another popular program was the Lukas program (BINGS and TINGS programmes), developed by Hans-Leo Lukas at the Max Planck Institut fur Metallforsung in Stuttgart [1977Luk], Germany, but this program has not been commercialised. The CALPHAD technique is used extensively in alloy development, as well as hardmetals (carbides), aqueous solutions, chemical vapour deposition and corrosion applications. It is also possible to apply the CALPHAD technique to model polymer solutions, though this is a relatively new application and suitable models are still in an early stage of development. Extensive databases have been developed for general as well as specific applications, with the most significant being the Science Group Thermodata Europe (SGTE) consortium's databases (www.sgte.org). Databases for alloy-specific applications, e.g. Ni-based superalloys, Al-alloys, solder and steels, have been developed by the relevant industry sectors. These databases are the result of CALPHAD optimisations.

Some of the software includes a module for the optimisation of the Gibbs energy functions, e.g. the Parrot module [1984Jan] in Thermo-Calc. Many databases have been developed for various commercial alloy systems. Conversion programs are also available to transport data from one system to another, although the current trend is to present data in the SGTE format, which can be used by all the programs.

The success of the CALPHAD technique is underwritten by the many application programming interfaces which are being developed to use the results from the equilibrium CALPHAD calculations in third party software programs like MatLab®. Major successes have been the combination of thermodynamics and kinetics to simulate diffusion transformations, e.g. DICTRA in Thermo-Calc and JMatPro, a software program developed by ThermoTech in the UK [2001Li], which uses thermodynamic and kinetic databases to predict material structures and mechanical properties. The Phase Field method is a new method under development, where the microstructures of alloys are simulated through equilibrium calculations based on the CALPHAD method. A commercial application program, MICRESS, has been released by ACCESS e.V. Solidification, solid-state transformations, grain growth and recrystalisation can be studied.

Evaluating recent literature, it is clear that the different modelling techniques are getting closer to each other and increasingly often data are extrapolated between the different methods. Themochemical and first principle (*ab initio*) values are becoming more comparable. It seems that most of the discrepancies which still exist are associated with cases where the postulated metastable allotrope is mechanically unstable to shear and will spontaneously collapse at 0 K [1988Pet]. Miedema's semi-empirical method is frequently used to generate enthalpies of formation for the assessments of systems where no experimental data are available. The CALPHAD thermodynamic assessments also have been successfully performed using a CVM approach to describe the lattices [1990Sun].

One of the major obstacles in the marriage of the different thermodynamic modelling techniques, however, still remains the extrapolation of sets of data between the CALPHAD technique and *ab initio* modelled systems, as the data are incompatible and the conversions

are complex. This limits the use of data from one technique to another to the use of individual values for constituents, substances and phases.

5.4 CALPHAD Methodology

The CALPHAD technique fits experimental data on the phase equilibria, thermochemical information on the separate phases and physical information of the elements, constituents and phases through a mathematical regression process to Gibbs energy curves. One of the most significant advantages of this methodology is that, because a total Gibbs energy is calculated, all the associated functions (heat capacities, enthalpy, activity, chemical potential, etc.) and characteristics of phase equilibria (phase diagrams, potential diagrams, Scheill diagrams, etc.) can be derived.

The standard methodology of a CALPHAD type assessment is illustrated in Figure 5.1. The procedure defines three different stages: first the literature is critically evaluated and models are proposed for the different phases in the system. Secondly, the Gibbs energies are calculated and re-calculated, in an iterative process, continuously comparing the calculated result with the experimental data, until the final stage, where a workable description is obtained such that it satisfies the application requirements. These stages will be discussed in broad terms to provide an understanding of the principles involved. For more detailed information, the reader is referred to the optimiser program's manual, 'CALPHAD - A comprehensive Guide' by Saunders and Miodownik [1998Sau] and some general and practical optimisation guidelines by Kumar and Wollants [2001Kum].

A thorough literature review of the experimental data of the alloy system to be assessed is essential. Data that can be used for an assessment includes experimental phase diagram data and thermodynamic data. Experimental phase diagram data can be invariant reactions, phase compositions and composition ranges, liquidus temperatures and crystal structure information. Thermodynamic data can be experimental, calculated with *ab initio* methods or predicted by empirical models. Enthalpies of formation, activity data, chemical potentials, differential thermal analysis (DTA) and differential scanning calorimetry (DSC) results, etc. can be used. *Ab initio* methods have proved to be successful in providing data for cases where there are no data available. Predictions, like Miedema's semi-empirical model, are useful to estimate enthalpies of formation, especially when the necessary experiments cannot be performed due to adverse conditions necessary, for example, very high temperatures or very reactive compounds.

The data must be evaluated for accuracy, reliability and consistency. Different types of data have different accuracies associated with them. For instance, composition analysis can be performed by analytical chemistry, microprobe analysis or X-ray energy dispersive analysis (EDS) with or without standards, in the scanning electron microscope. Chemical analysis using a primary method will produce much more accurate results than standardless EDS analysis. Thermodynamic data from DTA are affected by whether a heating or cooling cycle has been used for the calculations. It is thus important to not just rely on review articles, but to scrutinise the original publications to objectively evaluate the data. According to the accuracy, reliability and consistency of the data, relative weights are assigned to the data during the CALPHAD optimisation. Unreliable and inconsistent data should not be included in the optimisation.

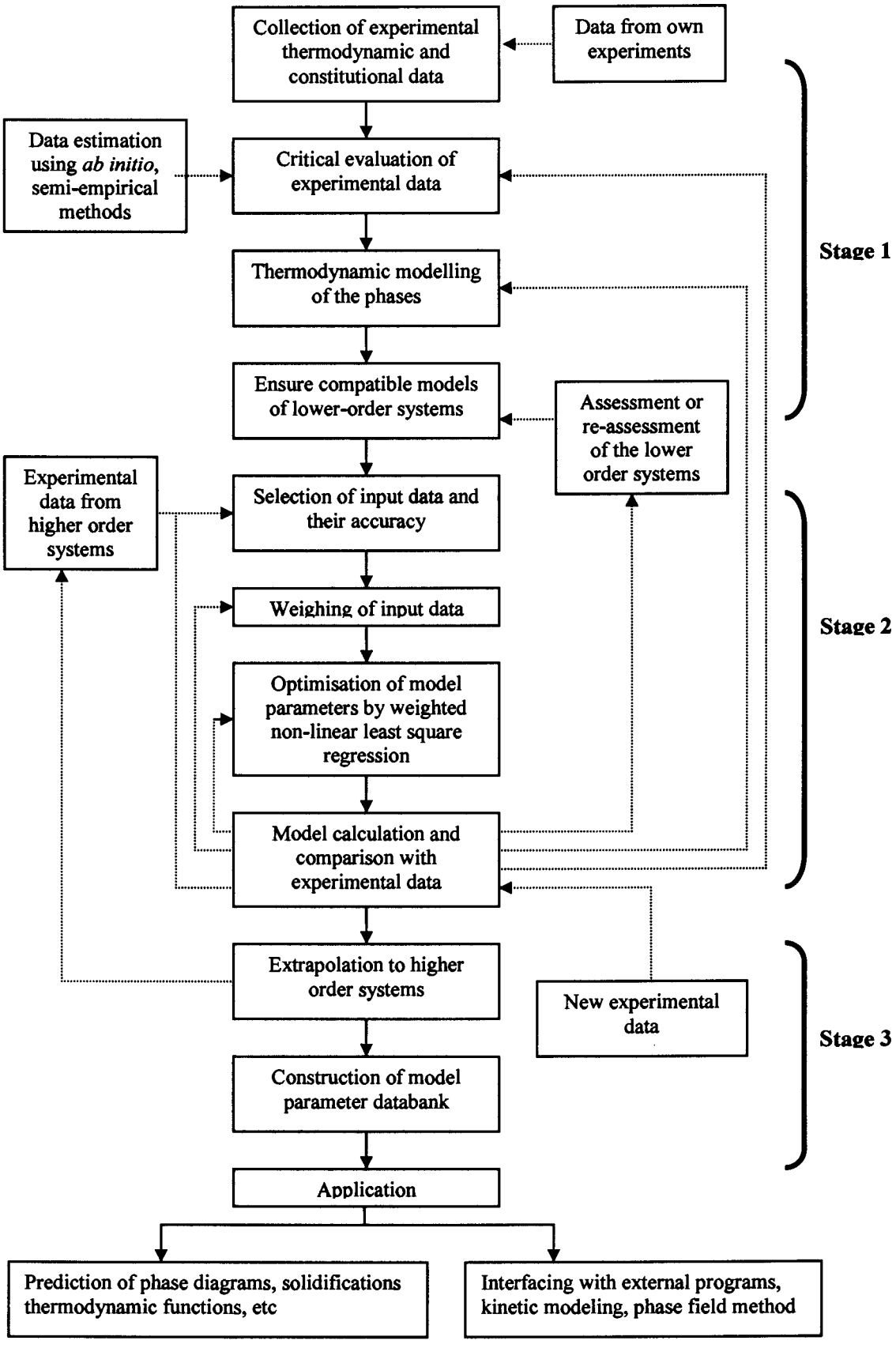

Figure 5.1. Flowchart of the CALPHAD method, adapted from [2001Kum].

The data can be compiled as a set of equilibrium data-points in the system. Each data-point is such that there are zero degrees of freedom in the phase rule

$$F = C - P + 2$$

where F is the degrees of freedom, C is the number of components and P is the number of phases.

A measurement error associated with the equilibrium data-point must be determined. Each equilibrium data-point contains dependent and independent quantities. The dependent quantity of each data-point must fulfil the phase rule, since it will be calculated in the optimisation. Thus it is important, when extracting data from, for example phase diagrams, that care is taken as to whether the composition or temperature is set as the dependent quantity. This is illustrated in Figure 5.2. For a steep slope on a phase diagram, a larger error is associated with the temperature than with the composition, so the composition should be the dependent value, as it has a smaller error in comparison the error associated to the temperature value, so that the smallest value contributes with the sum of squares in the optimisation.

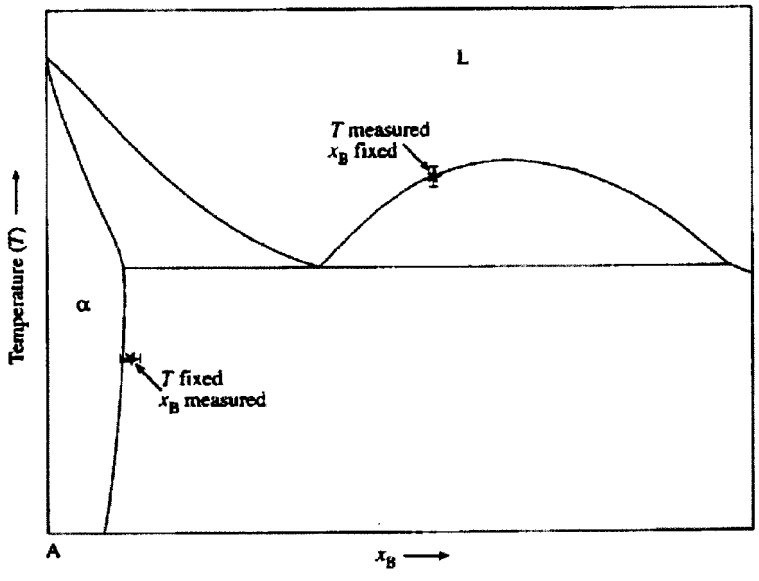

Figure 5.2. Phase diagram showing regions where only composition can be reliably measured at a given temperature and vice versa [2001Kum].

A reference state must be established for each element or component. This is generally taken to be the crystal structure in which the element exists at standard temperature and pressure. For consistency, and to allow extrapolations between different calculated systems, the reference state as prescribed in the SGTE database is usually referred to.

An important factor in the calculation of the Gibbs energy curves for a phase or system is the selection of the models that are used to describe the phases. Although the models are not strictly based on the crystal structures, some consideration should be given to the crystal structure and the model must have some physical meaning in describing the phase as for example a stoichiometric compound, an ordered phase or as a solid solution phase. Homogeneity ranges in a phase are normally due to defects (either anti-site atoms - atoms occupying the 'wrong site' - or vacancies) in the ideal structure of the phase. In most cases, the types of defect are not known and then a general approach can be applied adding the defects

on an additional lattice. However, care must be taken to select a suitable, simple and robust model, especially if the data are needed for extrapolation into higher order systems, as complex models are difficult to handle by the software and can lead to problems when extrapolated. Where possible, the model must follow 'standardisation' to ensure consistency, for instance the order/disorder transformations and structure relations of bcc-A2/B2 and fcc-A1/$L1_2$. Although there are good references available in the literature for some specific models [2001HilC, 1999Dup], models are constantly refined and changed as knowledge and understanding of the phase and its behaviour increases.

The assessments in this study were performed with the Parrot module [1984Jan] in the Thermo-Calc software [1985Sun]. Parrot is a program for the evaluation of thermodynamic model parameters from experimental observations of quantities describing a set of equilibrium states of the system. The model parameters are estimated by a weighted non-linear least squares optimisation of thermochemical and constitutional data.

5.5 CALPHAD Thermodynamics

5.5.1 Some basic principles

The CALPHAD method is based on Gibbs free energy functions. The state of a system can always be described in terms of the Gibbs free energy, since a system always tries to minimise its energy by minimising its enthalpy while maximising its entropy at constant pressure Thus, the Gibbs energy is the most fundamental way to describe a system in terms of its energy status.

The Gibbs energy is always given related to some reference, since for many elements more than one structure is stable, depending on the temperature and pressure. In the CALPHAD method, the state of the element that is stable at 101 325 Pa and 298 K is usually selected as the reference state.

Data must be kept consistent, that is, refer to the same reference states and have the same mathematical polynomial formalisms, in order to allow interchanging data with other data as well as to extrapolate data from various assessments to higher order systems. This study complies to the format of the Science Group Thermodata Europe (SGTE). All reference data for elements in this work is from Dinsdale [1991Din], who published a unified database under the auspices of SGTE.

5.5.2 Thermodynamics of Pure Elements

The Gibbs free energy G[P,T] of a pure element is given by the equation

$$G_{[P,T]} = H_{[P,T]} - TS_{[P,T]} \qquad (5.1)$$

where $H_{[P,T]}$ and $TS_{[P,T]}$, respectively, are the enthalpy and entropy as a function of temperature and pressure. These data are obtained from the SGTE database [1991Din]. The SGTE format for a pure element *i*, at constant atmospheric pressure, is

$$GHSER_i = G_{m[T]} - H_m^{SER}(298.15K) = a + bT + cT\ln(T) + \Sigma d_n T^n \qquad (5.2)$$

$$(\Sigma d_n T^n = dT^2 + eT^3 + fT^{-1} + gT^7 + hT^{-9}) \quad (5.3)$$

The left-hand side of the equation is defined as the Gibbs energy relative to a standard element reference state (SER) where H_m^{SER} is the enthalpy of the element in its defined reference state at 298.15 K; a, b, c and d_n are coefficients and n represents a set of integers, typically taking the values of 2, 3, -1, 7 and -9. The terms T^7 and T^{-9} have been introduced to remove the possibility of phases becoming incorrectly stable at high or low temperatures, respectively. The equation can be expanded to include terms to describe pressure and magnetic dependence. These effects are not relevant to the elements (Al, Pt and Ru) in this study.

The first and second derivatives of GHSER with respect to temperature are related to the absolute entropy and heat capacity of the element at the same temperature. This means experimentally determined heat capacity values can be used directly and the coefficients will be related to c, d, e, f, g and h.

This convention is convenient since all the data in a database, stored relevant to the SGTE reference state, are inter-consistent and can be combined to calculate chemical and metallurgical equilibria.

5.5.3 Thermodynamics of solutions

In CALPHAD, a solution phase is defined as any phase in which there is a range of solubility of more than one component. On atomistic scale, solutions consist of a mixture of different species, in the simplest case atoms. Solutions can be classified as substitutional solutions, sublattices, ionic, aqueous or polymers/organic molecules, and for the first four, specialised models have already been developed. The models for substitutional solutions and sublattices will be discussed in detail since they are relevant to metallic alloy systems. Although metallic alloy systems are referred to as solid solutions in physical metallurgy, the general terminology 'solution' will be used here as more than just metallic alloy systems can be described as 'solutions' in CALPHAD models described below.

The format for solutions is the same as the SGTE format used for pure elements (Equations 5.2 and 5.3). However, in most cases only the terms $a + b\ T$ are used. The term $T\ ln\ T$ is usually only used in cases where heat capacity data are available, which depicts the use of this term to ensure the correct derivation of the heat capacity from the Gibbs energy.

For all solution phases, the Gibbs energy is given by the general formula

$$G = G^{ref} + G^{id} + G^{xs} \quad (5.4)$$

where G^{ref} is the contribution of the pure compounds of the phase to the Gibbs energy, G^{id} is the ideal mixing contribution and G^{xs} is the contribution due to non-ideal mixing, also known as the Gibbs excess energy of mixing. G^{ref} for a system with N pure elements is obtained from

$$G^{ref} = \sum_{n=1}^{N} {}^0G_i^{ref} \quad (5.5)$$

where ${}^{0}G_i^{ref}$ is the Gibbs energy of i for the reference state obtained from the SGTE database.

5.5.3.1 Substitutional Solutions

A random substitutional approach is used for phases such as the gas phase or simple metallic liquid and solid solution phases where components can mix on any spatial position which is available in the phase. For instance, in a simple bcc phase of two bcc components, any of the components can occupy any of the atomic sites that define the cubic structure. In a gas and liquid, the crystallographic structure is lost, but otherwise positional occupation of the various components relies on the random substitution rather than any preferential occupation of a site by any particular component. Randomness can only be assumed as long as the species, atoms or molecules are sufficiently similar in size, shape, electronegativity, etc.

In evaluating simple mixtures, **ideal solutions** follow Raoult's law, i.e. the activity of an element i in the solution is equal to its mole fraction at all compositions as the bond strength between A and B are so similar that A and B are randomly distributed. Gases tend to follow ideal behaviour. However, in real A-B solutions, the interaction between A and B is different from that between A and A or B and B. Due to these attractive or repulsive forces, there will not be a random distribution of the compounds in the solution. The Gibbs energy of an ideal solution is

$$G_m = \Sigma x_i G_i^{\circ} + RT\Sigma x_i \log_e x_i \qquad (5.6)$$

where G_i° defines the Gibbs energy of the phase containing the pure component i. x_i is the mole fraction of component i. Ideal solutions do not have an excess energy contribution associated with them.

Some solutions exhibit random mixing, but the net heat absorbed or released is not zero ($H^M \neq 0$). This is called a **regular solution**. For a regular solution, an excess energy is needed and this is described with the excess energy G^{xs} term.

The excess energy G^{xs} can be expressed as $x_A x_B L_{AB}$, where L_{AB} is the interaction parameter as defined by Hildebrand [1929Hil]. The physical meaning of L_{AB} can be described as follows: When one considers the magnitude and sign of the interactions between the components in the phase that will have an influence on the total energy, but assumes that it is composition independent and further assumes that the total energy arises from only nearest-neighbour bond energies, the total energy becomes

$$\mathrm{E}_o = \omega_{AA}\mathrm{E}_{AA} + \omega_{BB}\mathrm{E}_{BB} + \omega_{AB}\mathrm{E}_{AB} \qquad (5.7)$$

where ω_{AA}, ω_{BB}, ω_{AB}, E_{AA}, E_{BB} and E_{AB} are the number of bonds and their energies associated with the formation of different bond types AA, BB and AB respectively. Assuming the reference states of pure A and B and that the bond energies are temperature dependent, it is then deduced that

$$G_m = \sum x_i G_i^{\circ} + RT\sum x_i \log x_i + \sum\sum x_i x_j L_{ij} \qquad (5.8)$$

with L_{ij} the temperature dependent interaction parameter between species i and j. For an ideal solution, the last term falls away as $x_i x_j$ becomes zero for pure i as well as pure j (Equation 5.6).

Since the regular solution model is composition independent, Kaufman and Bernstein developed the model further to include composition dependence and proposed the **subregular model**. In this model, interaction energies are considered to change linearly with composition and the Gibbs excess energy can be expressed as

$$G_{mix}^{xs} = x_i x_j (L_{ij}^i x_i + L_{ij}^j x_j) \tag{5.9}$$

The subregular model can be expanded to more complex composition dependencies in terms of a power series. The Redlich-Kister expansion is the most commonly-used expansion and the Gibbs energy for a substitutional solution can then be rewritten as

$$G_m = \sum x_i G_i^\circ + RT \sum x_i \log x_i + \sum_i \sum_{j>i} x_i x_j \sum_\nu (x_i - x_j)^\nu L_{i,j}^\nu \tag{5.10}$$

where the temperature dependence of the interaction parameter can be described as

$$L_{i,j:i} = y_i' y_j' [a_0 + b_0 T + c_0 T \ln T (a_1 + b_1 T)(y_i' - y_j')] \tag{5.11}$$

The index ν denotes the regularity of the solution, L^o is designated for the regular solution, L^1 is referred to as the subregular solution parameter and L^2 the subsubregular solution parameter.

Equation 5.10 is usually used to describe metallic systems for substitutional phases and to describe a disordered solution such as liquid, fcc, bcc and hcp.

5.5.3.2 Sublattice Model / Compound Energy Formalism

The above-mentioned models fall short in accurately extrapolating to higher solute contents or extending the description to higher order alloy systems for phases which display some form of order. As the CALPHAD approach sometimes needs to evaluate or estimate unknown, unstable and/or metastable phases and stoichiometric compounds, a sublattice model (SL), also designated the Compound Energy Formalism (CEF), has been developed [1970Hil, 1945Tem, 1981Sun]. This model can be envisaged as interlocking sublattices on which the various components can mix. Although the model does not define any crystal structure, internal parameter relationships can be defined with respect to different crystal structures, such as the order-disorder transformation. This is now one of the most commonly-used methods to describe solution and compound phases because it is flexible and can account for a variety of different phase types (e.g. interstitial phases, intermetallics, σ, μ). In simplified form, this model can also describes stoichiometric line compound phases where each sublattice is occupied by a single type of atom, and substitutional solution phases which contain only one sublattice. To be in line with modern literature on sublattice modelling, the term 'Compound Energy Formalism' (CEF), will be used.

The physical meaning of the sublattice model for the system $(A,B)_1(C,D)_1$ has been schematically described by Saunders and Miodownik [1998Sau] with a composition space and reference energy surface, as illustrated in Figure 5.3.

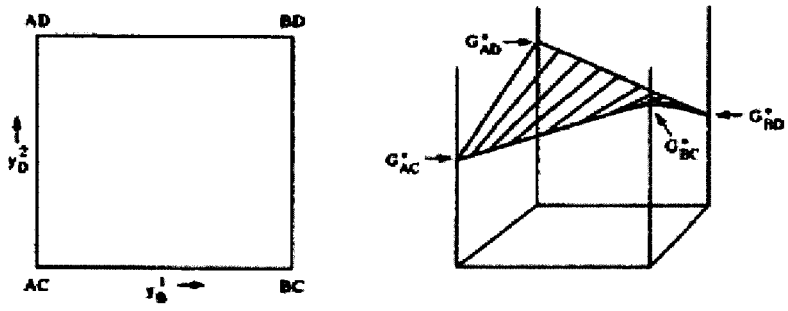

Figure 5.3. Composition space and reference energy surface for $(A,B)_1(C,D)_1$ [1998Sau].

All possible compositions in the system are encompassed by the composition space AC-AD-BD-BC. These four compounds at the corners of the composition space are the so-called 'end-members'.

The reference energy surface can be represented by the equation

$$G^{ref} = y'_A y''_C G^{\circ}_{A:C} + y'_A y''_D G^{\circ}_{A:D} + y'_B y''_C G^{\circ}_{B:C} + y'_B y''_D G^{\circ}_{B:D} \qquad (5.12)$$

The Gibbs energies of the compounds AC, BC, AD and BD control the interactions A-C, A-D, B-C and B-D respectively. Mixing on the sublattices controls A-B and B-D interactions and the simplest form of interaction is a regular solution format such that

$$G^{xs} = y^1_A y^1_B L^0_{A,B:*} + y^1_C y^1_D L^0_{*:C,D} \qquad (5.13)$$

where $L^0_{A,B:*}$ and $L^0_{*:C,D}$ denote regular solution parameters for mixing on the sublattices irrespective of the site occupation of the other sublattice and '*' denotes that the sublattice is independent of the constituent on that sublattice. Equation 5.13 is composition independent. However, the interactions can be composition dependent and the excess energy is then described with a subregular model (Equations 5.10 and 5.11).

According to the sublattice model developed by Sundman and Ågren [1981Sun], an intermetallic phase can be described as

$$(A_{y'_A} B_{y'_B} ....)_p (C_{y'_C} D_{y'_D} ....)_q ..... \qquad (5.14)$$

where the species A, B... can be atoms or vacancies. p and q are the number of sites, y'_i and y''_j are the respective site fractions of species i and j in their respective sub-sublattices, designated by ' and ". Each sublattice (s) has the condition $\sum_i y_i^s = 1$. When $p + q + ... = 1$, the thermodynamic quantities are referred to as one mole of sites.

The Gibbs energy of mixing for a sublattice phase is

$$G_m = G^{ref} + G^{id} + G^{xs} \tag{5.15}$$

The components of Equation 5.15 are expanded as follows [1981Sun]:

$$G^{ref} = y'_A y''_C G^{\circ}_{A:C} + y'_A y''_D G^{\circ}_{A:D} + y'_B y''_C G^{\circ}_{B:C} + y'_B y''_D G^{\circ}_{B:D} \tag{5.16}$$

$$G^{id} = RT[p(y'_A \ln y'_A + y'_B \ln y'_B) + q(y''_C \ln y''_C + y''_D \ln y''_D)] \tag{5.17}$$

$$G^{xs} = y'_A y'_B [y''_C L_{A,B:C} + y''_D L_{A,B:D}] + y''_C y''_D [y'_A L_{A:C,D} + y'_B L_{B:C,D}] + y'_A y'_B y''_C y''_D L_{A,B:C,D} \tag{5.18}$$

$G^{\circ}_{A:B}, G^{\circ}_{A:D}, G^{\circ}_{B:C}$ and $G^{\circ}_{B:D}$ represent the Gibbs energy of formation of the stoichiometric compounds A_pC_q, A_pD_q, B_pC_q and B_pD_q, which might be stable, metastable or even unstable in the system. y_i^s is the site fraction of element i on sublattice s. In Equation 5.18, L is the interaction parameter and expressed as a function of temperature $L = a + b*T$.

For the special case where order-disorder relationships exist between phases in a system, the Gibbs energy can be described as [1998Ans]:

$$G_m = G_m^{dis}(x_i) + \Delta G^{ord*}(y'_i y''_i) - \Delta G^{ord*}(x_i, x_i) \tag{5.19}$$

where $G_m^{dis}(x_i)$ is the molar Gibbs energy contribution from the disordered state and $\Delta G_m^{ord}(y'_i; y''_i)$ is the ordering energy contribution, equal to zero in the disordered state and $\Delta G^{ord*}(x_i, x_i)$ represents the extraneous excess energy contribution from the ordered parameters when the phase becomes disordered.

The power of the sublattice model lies in the fact that many of the other models, like the substitutional solution model, are simplifications of the SL/CEF. On the other hand, the model can be specifically applied to a complex ordered crystal structure, like sigma phase, or used to describe order-disorder relations between similar phases, like the γ/γ' in Ni-based super alloys. Some of the applications of the CEF are listed in Table 5.1.

Table 5.1. Applications of the compound energy formalism.

Phase	**Description**
Stoichiometric Compound	$(A)_a(B)_b$
Interstitial Solutions	$(Fe,Ni)_p(C,N,Va)_q$
Substitutional Solutions	$(A_{x1},B_{x2},C_{x3},...)$
Ordered Phase (ie Ni_3Al -$L1_2$)	$(Al,Ni)_{0.25}(Al,Ni)_{0.25}(Al,Ni)_{0.25}(Al,Ni)_{0.25}$
Ordered Phase (e.g. Ru_2Al_3)	$(Al)_3(Al,Ru)_2(Ru,Va)$
Salt Mixtures	$(A^+,B^+)_a(C^-,D^-)_b$
III-V compounds	$(A^{III},B^{III})_A(C^V D^V)_b$
Liquid Ionic solution	$(Al^{+3})_p(O^{-2},SiO_4^{-4})_q$

A number of custom two-, three- and four-sublattice models have been developed to describe additional parameter relations in certain order-disorder transformations. These models ensure consistency and data compatibility in the descriptions from different researchers and allow the

data to be extrapolated to higher order systems without adjusting the phase descriptions. The application of the CEF to fcc and B2 ordering will be discussed as in the Al-Pt-Ru system.

Hillert [2001Hil] recently published a comprehensive review article on the compound energy formalism. It was accompanied by an applications article by Frisk and Selleby [2001Fri], which will give the reader more insight into CEF modelling.

5.5.3.2.1 CEF applied to B2/A2 order/disorder transformation

The disordered format of the B2 phase (CsCl-type) is the A2 phase (W-type). Figure 5.4 presents schematic diagrams of both structures. The B2 phase can be seen as two interpenetrating primitive cubic sublattices and in the completely ordered crystals (ideal case) the positions of the first sublattice, α, are occupied by atoms of kind A and the other sublattice, β, by atoms of kind B. In the A2 structure, all the sites are equivalent and the structure is called disordered. Disordering reactions have been experimentally observed as first or second order.

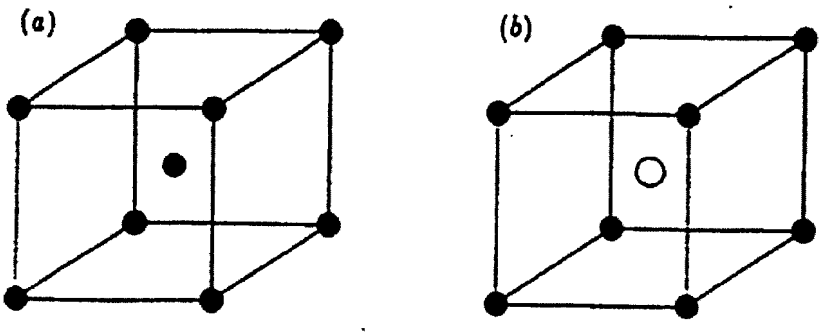

Figure 5.4. Schematic crystallographic structure of the A2 and B2 phases. (a). A2, the disordered structure, where all the sites are equivalent. (b) B2, the ordered structure where the occupation of the site in the centre of the cube is different to the one on the corner.

Phases with the B2 structure are generally formed around the equiatomic composition in binary systems and are often characterised by a considerable homogeneity range. In many cases, they remain ordered to high temperatures, and normally melt congruently. The deviations from the stoichiometric composition AB are possible by formation of statistically distributed point defects (so-called constitutional defects). Four basic kind of defects can occur in a crystal of the CsCl type (interstitial positions are not considered)

(i) A atoms on the β sublattice;
(ii) B atoms on the α sublattice;
(iii) vacancies on the α sublattice or
(iv) vacancies on the β sublattice.

The first two defects are called the anti-structure atoms. Traditionally, the B2 phases are divided into two groups according to the predominant defect mechanisms, the first group is dominated by anti-structure atoms (also called substitutional type) while the second group is dominated by vacancies on the α sublattices with A atoms on the β sublattice. The latter is called the triple defect, as two vacancies are needed to balance one anti-structure atom on the

other lattice. In only some B2 structures the defect mechanisms have been identified. In the modelling of the B2 phases, these defect structures have to be considered. This could be quite troublesome when the defect mechanism is not known and assumptions must be made. This has also lead to the use of different models to describe the B2 phase. Problems arose when different models were used and higher order systems had to be extrapolated.

Two CEF models have been used in the past to describe the B2 phase, where for a simple binary case, it can be described as

(A,B)(A,Va) or (A,B)(A,B)

Due to the different defects assumed, the models are incompatible and complex and cumbersome conversions are required to make the models equivalent.

A modification of the traditional two-sublattice model has been introduced by Dupin and Ansara [1999Dup]. It is called the Modified Sublattice Model (MSL) and considers all defects simultaneously in a symmetrical description of the B2 phase

$$(A,B,Va)_{0.5}(A,B,Va)_{0.5}(Va)_3 \qquad (5.20)$$

This description is mathematically equivalent to the previous models. The mathematical conversion between the different models has been reported by Dupin and Ansara [1999Dup]. In the light of this modified model, Hillert and Selleby [2001Hil2] then suggested to treat all defects rather as point defects, as this simplifies the usage of the MSL model.

The MSL model introduces some constraints that must be met. As both lattices are identical, the Gibbs energy contribution of the ordered state is given by

$$G^{B2}_{Al:Ru:Va} = G^{B2}_{Ru:Al:Va} \qquad (5.21)$$

$$G^{B2}_{Al,Ru:Ru:Va} = G^{B2}_{Ru:Al,Ru:Va} \qquad (5.22)$$

In the case of the MSL the disordered state of the B2 phase is described by the bcc-A2 phase. However, when the MSL is used in an optimisation, certain parameters are not free and should not be optimised [1999Dup].

5.5.3.2.2 CEF applied to fcc ordering

The Pt_3Al phase is an ordered structure ($L1_2$) of the disordered fcc phase (A1), the latter in which the atoms are randomly distributed on the lattice. The Pt_3Al phase shows both long-range and short range order (*lro* and *sro* respectively).

A four sublattice compound energy formalism (4SL CEF) has been successfully used by Sundman *et al.* [1998Sun] to describe the order-disorder relationship in the $L1_2$, $L1_0$ and fcc-Al phases in the Au-Cu system, where they introduced the concept of reciprocal parameters to describe the short range order. Kusoffsky *et al.* [2002Kus] described the general principles of the CEF applied to fcc ordering.

In order to model the disordered fcc phase (A1) and the ordered fcc phases ($L1_0$ and $L1_2$) phase with a single model, it is necessary to consider four sublattices. Thus according to 4SL CEF, the fcc phases for the case Al-Pt can be described with the following model

$(Al,Pt)_{0.25}(Al,Pt)_{0.25}(Al,Pt)_{0.25}(Al,Pt)_{0.25}$ (5.23)

Physically, the sublattices describe the four corners of a tetrahedron in a unit cell, which are illustrated in Figure 5.5. Due to the crystallographic symmetry of the unit cell, the sublattices must be identical, implying that all nearest neighbours of an atom are on a different sublattice. With 0.25 sites for each sublattice, the requirement of 1 mole of atoms in the model is met. For the disordered structure (fcc_A1), all the sublattices are equivalent, which reduces this model to an equivalent (Al,Pt) substitutional model. When two sublattices have the same fractions, but are different to the other two which also have the same fractions, it describes the PtAl phase ($L1_0$ structure). When three sublattices have the same fractions and the fourth sublattice a different fraction, the above model describes the Al_3Pt and Pt_3Al phases ($L1_2$ structure). Not all four phases are necessarily stable in a system. $PtAl_3$ and Pt_2Al_2 are unstable in the Al-Pt system, i.e. they don't exist in any stable form in the Al-Pt system.

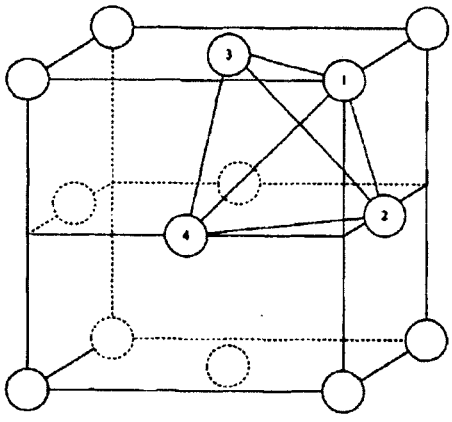

Figure 5.5. The face-centred cubic (fcc) structure. The numbers indicate the four sublattices for ordering.

From the model, the following relationships hold

$$\sum_i y_i^s = 1 \tag{5.24}$$

$$x_i = 0.25\sum_s y_i^s \tag{5.25}$$

with y_i^s the site fraction of each element i on each sublattice s and x_i the molar fraction of i.

The Gibbs energy expression describing the fcc phases is

$$G_m = \sum_i\sum_j\sum_k\sum_l y_i^{(1)}y_j^{(2)}y_k^{(3)}y_l^{(4)}{}^oG_{i:j:k:l} + 0.25RT\sum y_i^{(s)}\ln(y_i^{(s)}) + {}^EG_m \tag{5.26}$$

where the first term describes the mechanical mixing of all the stoichiometric compounds defined by the model, with ${}^oG_{i:j:k:l}$ being the Gibbs energy of the stoichiometric compound *ijkl* relative to the pure elements in the fcc state. The second term is the random mixing of all elements in each sublattice. The excess term ${}^EG_m$ includes the first two interactions according to the CEF model and is defined as

$$^{E}G_m = \sum_{i_1}\sum_{i_2}\sum_{j}\sum_{k}\sum_{l} y_{i_1}^{(r)} y_{i_2}^{(r)} y_j^{(s)} y_k^{(t)} y_l^{(u)} L_{i_1,i_2:j:k:l} + \ldots + \sum_{i_1}\sum_{i_2}\sum_{j_1}\sum_{j_2}\sum_{k}\sum_{l} y_{i_1}^{(r)} y_{i_2}^{(r)} y_{j_1}^{(s)} y_{j_2}^{(s)} y_k^{(t)} y_l^{(u)} L_{i_1,i_2:j_1,j_2:k:l} + \ldots \quad (5.27)$$

The comma "," separates interacting constituents on the same sublattice and the column ":" separates the sublattices. The first summation describes the regular interaction parameters, $L_{i_1,i_2:j:k:l}$, which represents interactions between i_1 and i_2 on sublattice r, when the other sublattices, s, u and t, are occupied by constituents j, k and l. This is the next nearest neighbour interactions.

The second summation is called the reciprocal parameters. It represents the interaction on two sublattices, r and s, simultaneously while the other two sublattices, t and u, are occupied by constituents k and l respectively. This describes the nearest neighbour interactions, thus introducing a component to describe *sro* in the model. As all the sublattices are equivalent, symmetry relations can be applied to reduce the number of independent parameters.

The 4SL-CEF described above is mathematically equivalent to the two-sublattice CEF (2SL-CEF, first introduced by Ansara *et al.* [198Ans] for the Al-Ni system, as $(Al,Ni)_{0.25}(Al,Ni)_{0.75}$. describing fcc-A1 and Ni_3Al simultaneously. The 2SL-CEF has been widely used to describe the order-disorder relation in fcc phases. However, the 4SL-CEF can describe all the related fcc phases, resulting in a simpler description for multi-component systems where many of the fcc phases are stable.

5.6 CALPHAD Optimisations

The optimisation is based on the calculation of the local equilibria for the data-points used with the set of parameters. This is done through a least-squares method. The success of the optimisation depends on a number of factors, which, if not considered, can result in a set of parameters which give totally wrong results when the calculation is completed, even though a minimum set of parameters have been obtained.

The success of an optimisation depends on:

1. the selected models,
2. the selected experimental data,
3. the number of model parameters,
4. starting values for the model parameters, and
5. the order in which the parameters are optimised.

The main difficulty in starting an optimisation, after selecting the models, parameters and experimental data, is to supply starting values for all the model parameters that are optimised. Often parameters of a similar system can be used as starting values. However, the optimisation can fail to calculate a corresponding value for the data-points with the given set of starting values.

Thus, it is generally best to start with a minimum set of data and first calculate only the liquid phase and the end members, e.g. fcc or hcp, of the system. It is also important to include thermodynamic data-points as they can be explicitly calculated from the Gibbs energy model,

unlike phase diagram data that are implicit and have to be calculated through solving non-linear equations. Once acceptable descriptions for these have been obtained, the phases can be introduced one by one. The results should regularly be evaluated against the experimental data by calculating the phase diagram for the phases that have been assessed.

The optimisation programs report a standard deviation for each parameter being optimised, and its meaning should be considered throughout the optimisation, since it is a measure of the significance of the parameter. A large standard deviation implies that the parameter is badly determined and should not be included in the optimisation. In such cases, a fixed value can be assigned to the parameter or the model should be changed.

5.7 Prediction of higher order systems

The usual strategy for assessment of a multi-component system is shown in Figure 5.6. First, the thermodynamic descriptions of the constituent binary systems are derived. Thermodynamic extrapolation methods are then used to extend the thermodynamic functions of the binaries into ternary and higher order systems. The results of the experiments are compared to the extrapolation, and if necessary, interaction functions are added to the thermodynamic description of the higher order system.

The coefficients of these higher-order system interaction functions are, similar to the binary case, calculated using experimental data and the CALPHAD method. In principle, this strategy is followed until all 2, 3,... n constituent systems of an n-component system have been assessed. However, in most cases, no corrections or very minor corrections are necessary for reasonable prediction of quaternary or higher component systems, as true quaternary phases are rarely found in metallic systems.

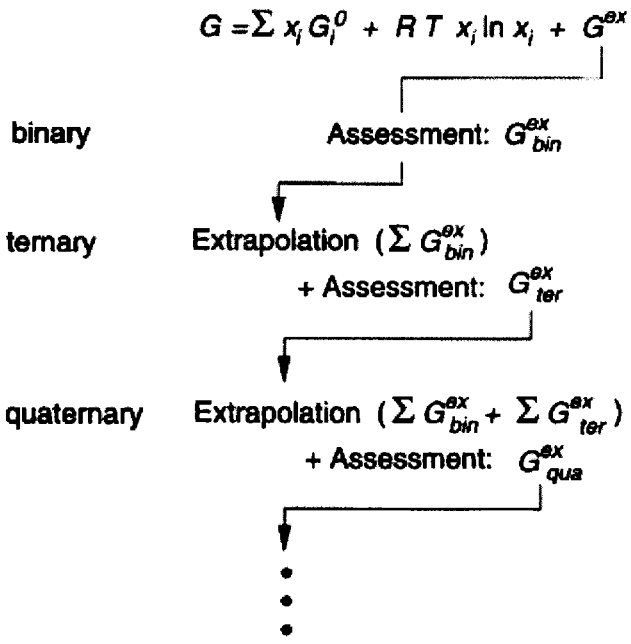

Figure 5.6. Extrapolation to higher order systems [1997Kat].

The results of such extrapolations can also be used to design critical experiments, saving the time and experimental cost to evaluate the complete system.

5.8 Conclusions

It has been shown above that computational methods can play an important role in materials science. Although the models used are simplified in comparison to real crystal structures, good approximations can be made of real systems. For some specialised cases, such as where order/disorder relationships exists between similar type of phases, specialised models have been successfully developed to address the relationships and simplify the calculations.

The CALPHAD method can be used to build databases that can predict the phase and property diagrams for a system. Where there is not enough data yet for accurate predictions, computational thermodynamics is a useful tool to critically design experiments.

Chapter 6
Results and Discussion of the Assessments

The Al-Ru, Al-Pt and Al-Pt-Ru phase diagrams were assessed with the CALPHAD method, using the Parrot module [1984Jan] in Thermo-Calc [1985Sun]. This chapter describes the models used in the assessments, the experimental data used and reports the modelled sets of parameters for the phases in each system. The Pt-Ru system has not been optimised. Instead, the existing description has been taken from Spencer's [1998Spe] noble alloy database, which is only an extrapolation of the elemental data.

As no textbook is available on the finer subtleties of optimisation, the optimisations are discussed in detail. The reasons for certain decisions are provided, as in many cases, model parameters are fixed by the user and not optimised. The reader is referred to the Thermo-Calc user's guide for information on the format of the data.

6.1 The Models

The success of an optimisation is based on the selection of sound models to describe the phase. Although the phase descriptions in the CALPHAD method are not strictly based on the crystallography of the phases, the crystallography can provide insight in how to model the phase. Certain phases, like the intermetallic B2 phase, are important in many related alloy systems and should be modelled to be consistent with previous descriptions to allow future combination of phase diagrams for extrapolation to higher order systems.

The models used in this study are listed in Tables 6.1 and 6.2 for the Al-Ru and Al-Pt systems respectively. A phase is called 'stoichiometric' when it is a line compound. Where the phase model was selected after a similar phase already modelled, it is referenced. Furthermore, in the phases where there are defects on the sublattices, instead of a separate set of parameters, only an enthalpy term was added in the calculation to compensate for the defect. Vacancies are indicated as Va.

Table 6.1. Thermodynamic models of the intermetallic phases in Al-Ru.

Phase	Model description	Model prototype	Reference	Comments
$RuAl_6$	$(Al)_6(Ru)$	$MnAl_6$		Stoichiometric
Ru_4Al_{13}	$(Al)_{0.6275}(Ru)_{0.235}(Al,Va)_{0.1375}$	Fe_4Al_{13}		Sublattice
$RuAl_2$	$(Al)_2(Ru)(Al,Ru,Va)$			Sublattice
Ru_2Al_3	$(Al)_3(Al,Ru)_2(Ru,Va)$	Ni_2Al_3		Sublattice
RuAl	$(Al,Ru,Va)_{0.5}(Al,Ru,Va)_{0.5}(Va)_3$ $(Al,Ru)(Al,Va)$	NiAl-B2* CoTi-B2**	[1997Ans] [2001Dav]	MSL Sublattice

Table 6.2 Thermodynamic models of the intermetallic phases in Al-Pt.

Phase	Model description	Model prototype	Reference	Comments
Pt_5Al_{21}	$(Al)_{21}(Pt)_5$			Stoichiometric
Pt_8Al_{21}	$(Al)_{21}(Pt)_8$			Stoichiometric
$PtAl_2$	$(Al)_2(Pt)$			Stoichiometric
Pt_2Al_3	$(Al)_3(Pt)_2$			Stoichiometric
PtAl	$(Al)(Pt)$			Stoichiometric
β	$(Al)_{0.48}(Pt)_{0.52}$			Stoichiometric
Pt_5Al_3	$(Al)_3(Pt)_5$			Stoichiometric
Pt_2Al	$(Al)(Pt)_2$			Stoichiometric
Pt_3Al	$(Al,Pt)_{0.25}(Al,Pt)_{0.25}(Al,Pt)_{0.25}(Al,Pt)_{0.25}(Va)$	$AuCu_3$	[1998Sun]	4SL CEF

The $RuAl_6$ phase is the only stoichiometric phase (line compound) in the Al-Ru system and the model is the simplified sublattice model for stoichiometric phases. Ru_4Al_{13} and $RuAl_2$ both have a composition range over which they are stable, but no data are available on the defects resulting in the composition ranges. Ru_4Al_{13} has been divided into 3 sublattices and modelled after the Fe_4Al_{13} phase [COST507], as the structure has been compared to Fe_4Al_{13} by Edshammer [1965Eds]. For $RuAl_2$, a sublattice has been added to accommodate the defects, only Va and Al atoms have been considered as defects as the phase width is more to the Al side of stoichiometry. Ru_2Al_3 is similar to the ordered Ni_2Al_3 and the description of Ansara *et al.* [1997Ans] was adopted. RuAl is a B2 phase with a very high degree of ordering throughout the temperature range that the phase is stable. Both vacancies and aluminium atoms have been suggested as defect mechanisms for this phase. In the sublattice description, the defect lattice contains Al and Va. The modified sublattice model (MSL) is completely symmetrical and the defects are only treated in selecting the model parameters which have to be calculated.

All the phases in the Al-Pt system, except for Pt_3Al, have been modelled as stoichiometric line-compound phases. According to the literature, the β phase is of the B2 type and has a composition range. The β phase has been simplified to a line compound, as no experimental or thermodynamic data are available. If data becomes available in future, the model can be changed without major impact on the overall set of parameters calculated for the system. The Pt_3Al phase has been described using the four-sublattice compound energy formalism (4SL CEF), suggested by Sundman [1998Sun] to treat the order-disorder relation in fcc structures (A1 and $L1_2$). To simplify the calculation, a functional approached is used for the 4SL CEF.

When the phases are modelled with different sublattices, the ratio of the sublattices can either be the stoichiometric ratios, or they can be defined as fractions so that the total number of sites adds up to one, so that the description describes one mole of atoms. In the first case, the parameters are then expressed as **J/mole**, while the latter is defined as **J/mole of atoms**. It is good practice to use only one of these methods, as mixing of the

methods can lead to confusion in the unit of the Gibbs energy for a phase. For example, the phase description for $RuAl_6$ can be (modified syntax)

```
ent-phase RUAL6   ,   2 6    1      AL ; RU ;   N N
G(RUAL6,AL:RU;0)=-156000+7*T+6*GHSERAL+GHSERRU ;
```

or

```
ent-phase RUAL6   ,   2 0.8571    0.1429      AL ; RU ;   N N
G(RUAL6,AL:RU;0)=-22286+T+0.8571*GHSERAL+0.1471*GHSERRU ;
```

where the first set gives the results in J/mole and the second set the results in J/mole of atoms, as the description is referring to one mole of atoms only. In this calculation of the Al-Ru system, both these descriptions had been used, while all sublattices were normalised to one mole in the Al-Pt system.

The Al-Pt-Ru phase diagram has only been extrapolated from the binaries; no ternary elements have been added to any of the intermetallic phases. A ternary assessment will only be possible when some thermodynamic data becomes available for the system. Ternary parameters would then probably have to be added to the liquid and fcc/$L1_2$ phases in the system. The optimisation of the ternary system falls outside the scope of this study.

The thermodynamic database for Al-Pt-Ru is listed in Appendix C, providing detailed descriptions of the phases.

6.2 Some basic concepts

The best approach to an optimisation with the Parrot module is to create a set-up file containing all the phase information, with variables for the model parameters that will be calculated. This is a text file with a .TCM extension and it is run with the 'macro' command in Thermo-Calc. Extra information can be entered into this file for future reference, model changes can be indicated allowing the user to keep track of the input and major phase compositions can be set to assist in the calculations.

To assist in the calculation of the ordered RuAl-B2 phase, a command setting the major composition was included, thus having Al on the first sublattice and Ru on the second. Only model parameters for the enthalpy contribution were set in the RuAl-B2 phase, the entropy contribution is described by the disordered bcc-A2 phase.

Experimental data are summarised in the POP file. The data are entered in 'equilibrium' sets. Each condition has its own data-set associated with it, and an example for the eutectic reaction L $\rightarrow$ (Ru) + RuAl at 2193 K and 70 at% Ru is provided here.

```
CREATE 1 1
SET-LABEL AINV
CHANGE-STATUS PHASE LIQUID HCP B2=FIX 0
SET-CONDITION P=1e5 T=2193:2
EXPERIMENT X(LIQUID,RU)=0.7:0.05
EXPERIMENT ORD≥0.9
SET-ALT-COND X(HCP,RU)=0.96
SET-ALT-COND X(B2,RU)=0.505
```

The conditions of the fixed phases, pressure and temperature fix the equilibrium. The 'experiment' is not an independent condition.

The ordering of the RuAl-B2 phase is important and a function

$$ORD = (Y(B2,Al\#1) - Y(B2,Al\#2))^2$$

was included in all the datasets containing the RuAl-B2 phase to ensure the RuAl-B2 phase is always ordered; this was met when ORD ≥ 0.7. The physical meaning of this is that the difference of the fraction of Al atoms on the first and Al atoms on the second lattice is calculated and when this is equal to one, the structure is fully ordered (only Al atoms on the one sublattice, and only Ru atoms on the second sublattice).

ALT conditions were added for when the optimisation is done in ALT mode. The ALT mode is discussed below.

Additional datasets were also added where negative driving forces were set to ensure the stability of a phase to lower temperatures. The Thermo-Calc POP files containing the datasets used in the optimisations are listed in Appendix D.

6.3 Assessment procedures

6.3.1 Al-Ru

The phase (Al) shows virtually no solubility for Ru, and on the phase diagram, (Al) forms through the eutectic reaction L → (Al) + $RuAl_6$ at < 0.01 at % Ru and 923 K, only 3 degrees lower than the melting point of pure Al. This implies that the slope of the liquidus must be negative at the temperature axis. So, as a first step, to ensure that the slope of the liquidus was correct at the melting point of the Al-fcc phase, only the liquid, Al-fcc and Ru-hcp phases were optimised. A metastable eutectic reaction was created for this purpose. This also ensured that the slope on the Ru-side is correct, though this would not have been a problem due to the high melting temperature of Ru and the fact that the eutectic L → (Ru) + RuAl occurs at 2193 K and 70 at. % Ru, about 414 K lower than the melting temperature of Ru.

However, when there is virtually no solubility of ruthenium in the (Al) solid phase, the slope of the liquidus surface is dependent on the enthalpy of melting. This means that the parameter cannot be effectively optimised and arbitrary values can be selected and fixed for the fcc phase. For fcc-A1, the interaction parameter $L^0_{Al,Ru}$ was set to -10 000 - 10*T from experience with other systems [2000Sun].

Once an acceptable liquidus slope was calculated, the RuAl-B2 phase, using the modified sublattice (MSL) formalism description, was included in the optimisation as this is the only phase with experimental thermodynamic data. This also gave the liquid phase a reference point. The bcc-A2 phase had to be introduced with the RuAl-B2 phase, as the bcc-A2 phase describes the disordered Gibbs energy contribution of the RuAl-B2 phase. The model parameters for the bcc-A2 interactions, where mixing with vacancies occurs ($L^0_{Al,Va}$ and $L^0_{Ru,Va}$), were set to a high positive value (80*T) as this prevents the stabilisation of the bcc-A2 phase due to excess vacancies in the RuAl-B2 phase.

The ALT mode in Parrot was used to determine the first model parameters, as the parameters initially were set to zero. The optimisation was continued in the normal mode once the ALT mode converged. The ALT mode is based on a 'reversal' of the normal model: the difference in chemical potential for each phase is calculated as the 'experimental information' and the program adjusts the model parameters to make the chemical potentials of all the phases the same, usually resulting in model parameters which can be successfully used as starting values in the normal mode. When the ALT mode is going to be used, extra information, such as the compositions of all the phases partaking in the equilibrium, should be included in the POP file.

An alternative to the ALT mode is to select starting values for model parameters from similar systems previously optimised. In a second optimisation, prompted at a later stage due to a model change, this approach was followed. There are many examples of the B2 phase, and the most well-known is probably the NiAl-B2 phase. However, the parameters from NiAl-B2 phase [1999Dup] could not be used, as NiAl-B2 has its phase extension to the Ni-rich side while RuAl-B2 has its phase width to the Al-rich side. TiCo-B2 has a similar phase shape as RuAl-B2, and the data from Davydov *et al.* [2001Dav] was used as a first estimation. In the initial optimisation, it was necessary to relax the ordering requirement to 0.7 until better model parameters were obtained.

The other phases, except for the Ru_2Al_3 phase, were introduced simultaneously. The liquid parameters were fixed while introducing the other phases into the calculation. These phases were introduced as stoichiometric congruent melting phases instead of the cascade of peritectic reactions by which they form in the phase diagram. This was done as congruent melting equilibria are easier to calculate than peritectic reactions. Once the phases were forming at the correct composition ranges in the calculated phase diagram, the peritectic reactions were introduced and the weights on the metastable congruent melting data were set to zero. The phase widths for Ru_4Al_{13} and $RuAl_2$ were only introduced after satisfactory results were obtained for the peritectic reactions.

Finally, the Ru_2Al_3 phase was introduced in a similar fashion as the above phases. The solid-state decomposition dataset was included at the end.

To ensure stability of the thermodynamic parameters of the intermetallic phases, a condition forcing the entropy of formation to be negative was set. The coefficients of the B2 and A2 phases were tested for interdependence and the entropy contribution of the ordered B2 phase is described by the disordered A2 phase. The interdependence testing was done by calculating the solubility range of the B2 phase as a function of the L(bcc-A2,Al,Ru) parameter. When the L(bcc-A2,Al,Ru) parameter is made more negative, the solubility range for B2 becomes wider, whereas when the G(B2,Al:Ru) = G(B2,Ru,Al) is made more negative, the solubility range becomes more narrow. Thus the parameters for the bcc-A2 phase could be fixed to give a reasonable solubility range for the B2 phase and the B2 parameters were optimised to adjust the solubility range.

The parameters were fixed through a rounding process. The parameter with the largest standard deviation was fixed with the number of significant numbers determined by the exponent of the standard deviation. The set of parameters was optimised again to ensure that the total sum of squares of error does not increase. This was repeated until only one value was left.

As the B2 phase can be described by either the MSL or the SL model, a second assessment was performed to obtain model parameters for the B2 phase using the SL model. The mathematical conversion model proposed for converting between MSL and SL parameters is not valid for the Al-Ru system as the bcc-A2 phase is unstable in this system, forcing some constraints on the MSL parameters [1999Dup].

For the SL optimisation, all the parameters calculated in the MSL optimisation were fixed. The description of the B2 phase was changed to the sublattice format. Only these parameters were optimised during the second assessment. The values from the TiCo-B2 phase [2001Dav] were used as starting values.

6.3.2 Al-Pt

The optimisation of Al-Pt was a re-assessment, as Wu and Jin [2000Wu] assessed the Al-Pt system. The re-assessment was considered to be necessary as their assessment did not describe the ordering in the Pt_3Al phase, and they also excluded the β and Pt_2Al phases from their optimisation due to a lack of experimental data on the phases. To be compatible with the latest order-disorder modelling of systems with a γ/γ' relation, the disordered fcc-Al and ordered Pt_3Al should be described using one Gibbs energy function. Furthermore, based on new experimental data [2000Big1, and this work], which were not available previously, the Pt_2Al and β phases have been confirmed and should thus be included.

The values reported by [2000Wu] were used as initial input values to the re-assessment. When their results were reproduced, the description for the fcc phases were changed to

the four-sublattice compound energy formalism (4SL CEF). In the 4SL CEF, the ordered Pt_3Al ($L1_2$ type fcc phase) and disordered fcc-A1 phases are described with one Gibbs energy function. The physical meaning of the 4SL CEF has been described in Chapter 5. In the Al-Pt system, only the fcc-A1 and Pt_3Al-$L1_2$ phases are stable, the $PtAl_3$-$L1_2$ and Pt_2Al_2-$L1_0$ phases are unstable. Pt_3Al forms congruently. Metastable congruent melting equilibria were introduced for the unstable phases, and a condition was set to suppress the phases in the diagram.

The Pt_2Al and β phases were also introduced initially by a metastable congruent melting as described in the Al-Ru system. The metastable conditions were removed and the peritectic reactions were introduced. The solid-state decomposition of the β phase was added in the final step. Although the literature [1986McA] suggests that the β phase has a B2 structure, it was decided not to model β as a B2 phase for a number of reasons. Firstly, the B2 phase descriptions are usually symmetrical around the 50:50 at. % compositions, thus a B2 phase description will have to be too far off the stoichiometry composition, suggesting excess defect formation in the phase. No data were available to confirm or contradict this. Secondly, because the β phase decomposes through a solid-state reaction at 1250 K, structural studies are extremely difficult. Thirdly, the PtAl phase is stable at 50:50 at. % in the system, with the Pt_2Al_2 phase from the 4SL CEF unstable at this same composition. Adding another phase at this composition would have complicated the optimisation too much. Also, the β phase (suggested to be the B2 structure) and RuAl-B2 phase are not continuous in the ternary system, so they can be modelled separately as simpler systems. It is usually better to model phases which are not continuous separately when a binary will be extrapolated to higher order systems.

6.3.3 Al-Pt-Ru

The Al-Pt-Ru phase diagram was predicted by extrapolation only from the three binary systems after the binary optimisations had been performed. However, thermodynamic parameters for the metastable descriptions of hcp-Pt, bcc-Pt and fcc-Ru were added from the SGTE database since all the metastable forms relevant to the system must be included in the description. Only the MSL B2 description version of the calculated Al-Ru system was used in the extrapolation.

Pt and Ru were added to the B2 and $L1_2$ phases respectively to stabilise these phases in the ternary system. B2 and $L1_2$ are both ordered phases and are described with one Gibbs energy function for the ordered and disordered forms of the phases, using the MSL model and 4SL CEF respectively. The inclusion of the third element to the disordered solutions (bcc and fcc respectively) requires the inclusion of the third element in the ordered phase as well. However, no parameters were included in the ordered descriptions for the third elements. No ternary interaction parameters were included for any phase in the system.

6.4 Results and discussion

6.4.1 Al-Ru

The calculated model parameters for the Al-Ru system are listed in Table 6.3. The calculated phase diagram is shown in Fig 6.1. The calculated phase diagram is compared with experimental data in Figure 6.2 and the invariant temperatures and compositions are compared in Table 6.4.

Table 6.3 Calculated thermodynamic parameters for the Al-Ru system [J/mol]

Liquid	Disordered Solution Phase: (Al,Ru)
	${}^{0}G_{Al}^{liq}(T) - H_{Al}^{0,fcc-A1}(298.15)$: [1991Din]
	${}^{0}G_{Ru}^{liq}(T) - H_{Ru}^{0,hcp-A3}(298.15)$: [1991Din]
	${}^{0}L_{(Al,Ru)}^{Liq} = -73000 - 14T$
	${}^{1}L_{(Al,Ru)}^{Liq} = -56000$
(Al) (fcc-A1)	Disordered Solution Phase: (Al,Ru)(Va)
	${}^{0}G_{Al}^{fcc-A1}(T) - H_{Al}^{0,fcc-A1}(298.15)$: [1991Din]
	${}^{0}G_{Ru}^{fcc-A1}(T) - H_{Ru}^{0,fcc-A1}(298.15)$: [1991Din]
	${}^{0}L_{(Al,Ru)}^{fcc\_A1} = -10000 - 10T$
(Ru) (hcp-A3)	Disordered Solution Phase: (Al, Ru)$(Va)_{0.5}$
	${}^{0}G_{Ru}^{hcp-A3}(T) - H_{Ru}^{0,hcp-A3}(298.15)$: [1991Din]
	${}^{0}G_{Al}^{hcp-A3}(T) - H_{Al}^{0,hcp-A3}(298.15)$: [1991Din]
	${}^{0}L_{(Al,Ru)}^{hcp\_A3} = -105000 + 30T$
bcc-A2	Disordered Solution Phase: (Al, Ru,Va)$(Va)_3$
	${}^{0}G_{Al}^{bcc-A2}(T) - H_{Al}^{0,bcc-A2}(298.15)$: [1991Din]
	${}^{0}G_{Ru}^{bcc-A2}(T) - H_{Ru}^{0,bcc-A2}(298.15)$: 26500-6.2*T+GHSERRU [1991Din]
	${}^{0}L_{Al,Ru:Va}^{bcc\_A2} = -176000 + 32 * T$
	${}^{0}L_{Al,Va:Va}^{bcc\_A2} = 120 * T$
	${}^{0}L_{Ru,Va:Va}^{bcc\_A2} = 120 * T$
$RuAl_6$	Stoichiometric Phase: $(Al)_6$ (Ru)
	${}^{f}G_{Al:Ru}^{RuAl_6} = 6{}^{0}G_{Al}^{fcc-A1} + {}^{0}G_{Ru}^{hcp-A3} - 156000 + 7 * T$
Ru_4Al_{13}	Sublattice Solution Phase: $(Al)_{0.6275}(Ru)_{0.235}$ $(Al,Va)_{0.1375}$
	${}^{f}G_{Al:Ru:Al}^{Ru_4Al_{13}} = 0.765{}^{0}G_{Al}^{fcc-A1} + 0.235{}^{0}G_{Ru}^{hcp-A3} - 35100 + 1.65 * T$
	${}^{f}G_{Al:Ru:Va}^{Ru_4Al_{13}} = 0.6275{}^{0}G_{Al}^{fcc-A1} + 0.235{}^{0}G_{Ru}^{hcp-A3} - 35100 + 1.65 * T$
$RuAl_2$	Sublattice Solution Phase: $(Al)_2$(Ru)(Al,Ru,Va)

$${}^{f}G^{RuAl_2}_{Al:Ru:Va} = 2{}^{0}G^{fcc-A1}_{Al} + {}^{0}G^{hcp-A3}_{Ru} - 136500 + 8*T$$

$${}^{f}G^{RuAl_2}_{Al:Ru:Al} = 3{}^{0}G^{fcc-A1}_{Al} + {}^{0}G^{hcp-A3}_{Ru} - 138000 + 8*T$$

$${}^{f}G^{RuAl_2}_{Al:Ru:Ru} = 2{}^{0}G^{fcc-A1}_{Al} + 2{}^{0}G^{hcp-A3}_{Ru} - 138000 + 8*T$$

Ru_2Al_3 Sublattice Solution Phase : $(Al)_3(Al,Ru)_2(Ru,Va)$

$${}^{f}G^{Ru_2Al_3}_{Al:Al:Va} = 5{}^{0}G^{bcc-A2}_{Al}$$

$${}^{f}G^{Ru_2Al_3}_{Al:Al:Ru} = 5{}^{0}G^{bcc-A2}_{Al} + {}^{0}G^{bcc-A2}_{Ru}$$

$${}^{f}G^{Ru_2Al_3}_{Al:Ru:Va} = 3{}^{0}G^{bcc-A2}_{Al} + 2{}^{0}G^{bcc-A2}_{Ru} - 312630 + 30.5*T$$

$${}^{f}G^{Ru_2Al_3}_{Al:Ru:Ru} = 3{}^{0}G^{bcc-A2}_{Al} + 3{}^{0}G^{bcc-A2}_{Ru} - 312630 + 30.5*T$$

RuAl (B2) Sublattice Solution Phase: (Al,Ru)(Al,Va)

$${}^{f}G^{B2}_{Al:Al} = 2{}^{0}G^{bcc-A2}_{Al}$$

$${}^{f}G^{B2}_{Al:Va} = {}^{0}G^{bcc-A2}_{Al} + 60000$$

$${}^{f}G^{B2}_{Ru:Va} = {}^{0}G^{bcc-A2}_{Ru} + 60000$$

$${}^{f}G^{B2}_{Ru:Al} = {}^{0}G^{bcc-A2}_{Ru} + {}^{0}G^{bcc-A2}_{Al} - 138700 + 15.5*T$$

$${}^{0}L^{B2}_{Al:Al,Va} = 49100 - 22.4*T$$

$${}^{0}L^{B2}_{Ru:Al:Va} = -51770 + 20*T$$

$${}^{0}L^{B2}_{Al,Ru:Al} = -30000$$

$${}^{0}L^{B2}_{Al,Ru:Va} = -30000$$

Modified Sublattice Model: $(Al,Ru,Va)_{0.5}(Al,Ru,Va)_{0.5}(Va)_3$

$${}^{f}G^{B2}_{Al:Al:Va} = 0$$

$${}^{f}G^{B2}_{Ru:Ru:Va} = 0$$

$${}^{f}G^{B2}_{Va:Va:Va} = 0$$

$${}^{f}G^{B2}_{Al:Ru:Va} = {}^{f}G^{B2}_{Ru:Al:Va} = -87600$$

$${}^{0}L^{B2}_{Al,Ru:Al:Va} = {}^{0}L^{B2}_{Al:Al,Ru:Va} = -73000$$

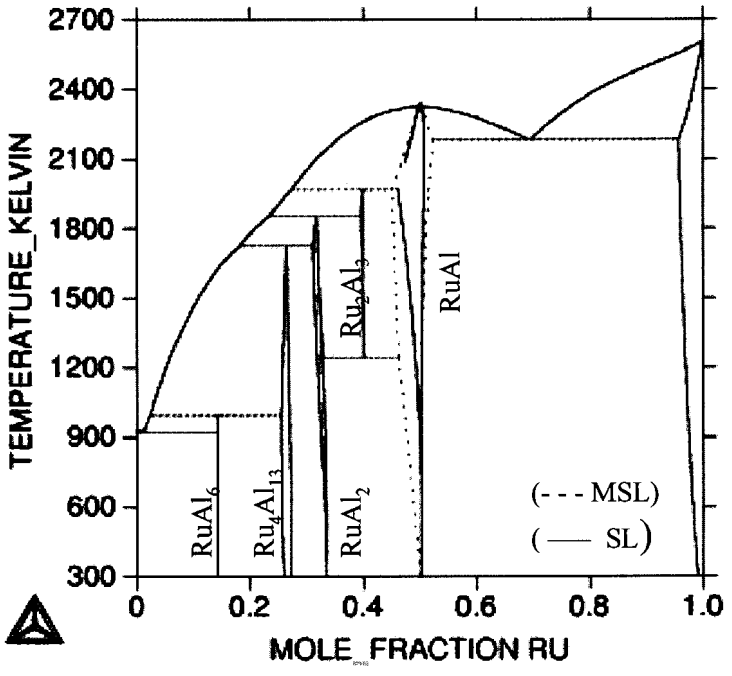

Figure 6.1 The calculated Al-Ru phase diagram showing RuAl-B2 calculated using the SL (—) and MSL (---) models.

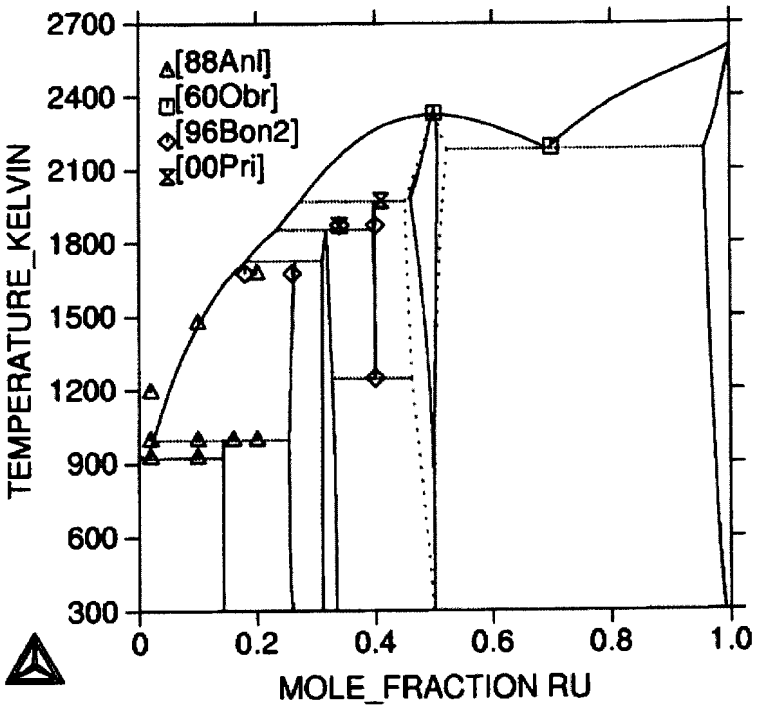

Figure 6.2 Comparison between the calculated Al-Ru phase diagram and experimental data from the literature (as listed in Table 6.4)

The calculated temperatures for the invariant reactions are in good agreement with the experimental temperatures, except for the peritectic formation of the Ru_4Al_{13} phase, which is about 50 K too high. This is probably due to the modifications to the invariant temperatures for the $RuAl_2$ and Ru_2Al_3 phases by Prins and Cornish [2000Pri] to correct the liquidus slope from the diagram of Boniface and Cornish [1996Bon2].

The homogeneity ranges of the Ru_4Al_{13} and $RuAl_2$ phases are acceptable in comparison with the experimental data. Ru_2Al_3 appears as a stoichiometric compound with no homogeneity range. The optimisation was simplified due to the lack of data for this phase and no interaction on any of the sublattices was taken into account, so effectively no defects were considered. The phase appears in the correct composition and temperature ranges and the description is considered satisfactory for the purpose of this work.

The two descriptions for the RuAl-B2 phase compare well, with the MLS description giving a better agreement to experimental data for the composition range. Both descriptions have a very limited extension to the Ru-rich side and correctly have the composition range to the Al-rich side.

Table 6.4 Calculated and Experimental invariant temperatures and compositions for the Al-Ru system.

Reaction (at. %Ru)							Reaction Temperature [K]	Reference
L	↔	(Al)	+	$RuAl_6$				
0.1		0		14.8			923	[1988Anl]
0.1		0		14.3			922	This work
L	+	Ru_4Al_{13}	↔	$RuAl_6$				
1.5		25		14.3			996	[1988Anl]
2.5		25.4		14.3			997	This work
L	+	$RuAl_2$	↔	Ru_4Al_{13}				
17.6		33.6		25.8			1676	[1988Anl]
18.1		31.1		26.7			1725	This work
L	+	Ru_2Al_3	↔	$RuAl_2$				
26		36		33.4			1733	[1996Bon1]
23		36.1		33.9			1873	[2000Pri]*
23.4		39.6		31.8			1854	This work
L	+	RuAl	↔	Ru_2Al_3				
33.5		42.5		42			1873	[1996Bon1]
27		42		41			1973	[2000Pri]*
35		45.9		39.9			1978	This work
Ru_2Al_3	↔	RuAl	+	$RuAl_2$				
395		46		35.9			1249	[1996Bon1]
40		49.5		32.9			1243	This work
L	↔	RuAl						
50		50					2333	[1960Obr]
50		50					2342	This work
L	↔	RuAl	+	(Ru)				
70		51		96			2193	[1960Obr]
69.7		50.7		95.7			2189	This work

* indicates values which was used for the optimisation.

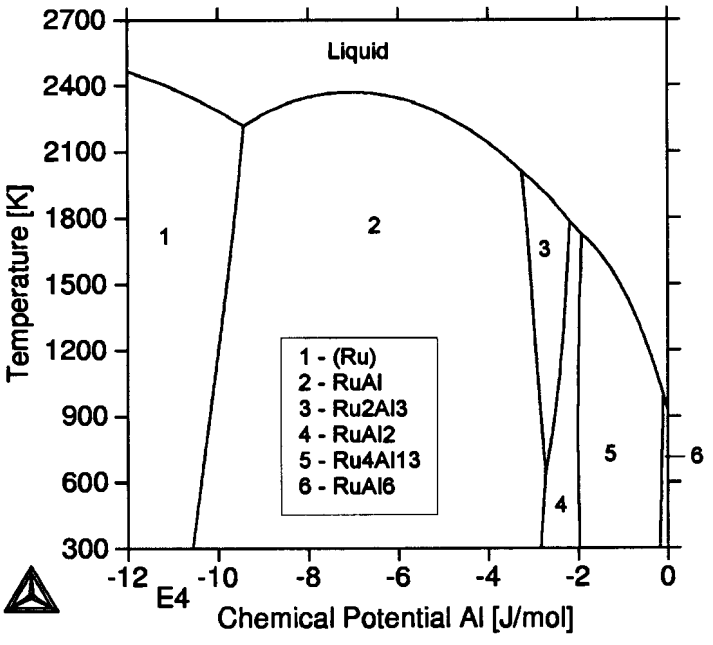

Figure 6.3. Phase diagram of temperature against chemical potential of Al.

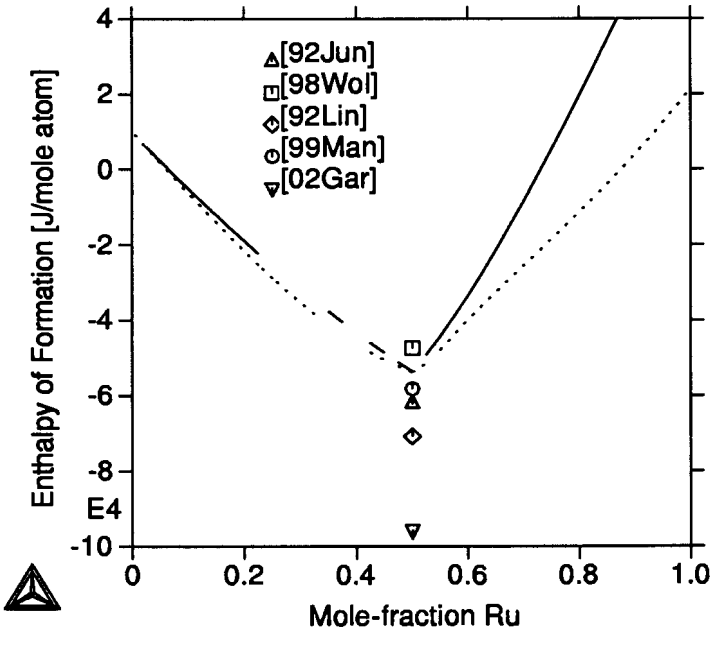

Figure 6.4. Comparison of calculated enthalpy of formation for the SL (—) and MSL (---) RuAl-B2 models with experimental results [1992Jun] and *ab initio* [1992Lin, 1998Wol, 1999Man, 2002Gar] predictions.

In Figure 6.3, the phase diagram is plotted as a function of the chemical potential of the Al instead of composition. The slope of the curves is equal to *dG/dT*, which represents the entropy. The diagram shows that no phase has an excessive entropy contribution, which is important as most of the thermodynamic data that was used in the optimisation was obtained by Miedema's semi-empirical method. In Figure 6.4 the enthalpy of formation for the sublattice and MSL descriptions of the RuAl-B2 phase is compared to experimental and ab initio values from the literature. The enthalpy of formation is in good agreement with the experimental value from Jung and Kleppa [1992Jun]. As expected, the MSL description resulted in a more symmetrical curve for the enthalpy of formation. For the sublattice description, the curve on the Ru-rich side of the 50:50 at. % composition indicates that the phase becomes more unstable at the higher Ru contents, which is in agreement with the non-symmetrical model.

6.4.2 Al-Pt

The calculated model parameters for the Al-Pt system are listed in Table 6.5. The optimised/calculated phase diagram is shown in Figure 6.5. The optimised phase diagram is compared with experimental data from the literature in Figure 6.6 and the invariant temperatures and compositions are compared in Table 6.6. The reactions for the PtAl, β and liquid phases are enlarged in Figure 6.7, as these are nearly indistinguishable on the full binary diagram.

The calculated compositions and temperatures for the invariant reactions for the intermetallic phases are in general good agreement with the experimentally reported compositions and temperatures. However, there are some areas in less good agreement, and in most cases it is due to the models being used.

The congruent formation of the Pt_3Al phase and $L \rightarrow Pt_3Al + (Pt)$ eutectic reactions are not in very good agreement with the experimental diagram, both reactions are shifted to lower platinum compositions in the calculated system. The 4SL CEF model is such that the formation composition of Pt_3Al is fixed at 75 at. %, while it has been reported in the literature to form congruently at 73.2 at. %. This off-stoichiometry formation cannot be described with the model, and had subsequently an influence on the temperature as well as the enthalpy of formation for the Pt_3Al phase. The symmetry and fixed compositions of the 4SL CEF model made it also impossible to move the eutectic reaction to lower Pt-contents. Furthermore, the phase area of the (Pt) solid solution is too narrow, especially at lower temperatures, but the phase area for the Pt_3Al phase is acceptable. However, the Pt_3Al phase is ordered throughout its phase area and the unstable $PtAl_3$ ($L1_2$) and Pt_2Al_2 ($L1_0$) phases, which are introduced through the 4SL CEF, are not stable at any composition or temperature in the phase diagram, which is correct.

Since the β-phase has been modelled as a line compound, with the stoichiometric composition fixed to the experimentally reported formation composition of 52 at% Pt, there are some discrepancies in the comparison of the calculated and experimentally reported compositions and temperatures. The formation composition and temperature are in good agreement with the value reported in literature, but the decomposition

composition is incorrect. The literature suggests the β-phase as an irregular phase area (see the Al-Pt phase diagram, Chapter 2, Figure 2.1), with the decomposition at higher platinum contents than the formation platinum content. This affected the calculated results for the reactions involving the β-phase. The calculated eutectic temperature for the $L \rightarrow \beta + Pt_5Al_3$ is ~50 K too high. This can also be due to the estimate of the enthalpy of formation for the β phase. The phase area is enlarged in Figure 6.7.

The Pt_5Al_3 phase forms experimentally through a peritectic reaction $L + Pt_3Al \rightarrow Pt_5Al_3$, which is very close to the liquid, it seems very close to a congruent melting reaction. The calculated Pt_5Al_3 phase forms congruently at 1750 K and 62.5 at. % Pt. This introduced an extra eutectic reaction $L \rightarrow Pt_5Al_3 + Pt_3Al$ at 1720 K and 67.1 at. % Pt, which is not observed in the experimental diagram.

On the Al-side of the phase diagram the (Al) shows a too high solubility for platinum. This is again due to the use of the 4SL CEF to describe the fcc phases. This also shifted the eutectic reaction $L \rightarrow (Al) + Pt_5Al_{21}$ to a too high Pt-content. As a result of the too high platinum solubility and the shift of the eutectic reaction, the liquidus is also too far too the right in comparison to results reported in the literature. However, the calculated results were accepted since the work is not aimed at studying Al-based alloys.

Table 6.5. The calculated model parameters for Al-Pt [J/mole of atoms].

Liquid	Disordered Solution Phase: (Al,Pt)
	$^0G_{Al}^{liq}(T) - H_{Al}^{0,fcc-A1}(298.15)$: [1991Din]
	$^0G_{Pt}^{liq}(T) - H_{Pt}^{0,hcp-A3}(298.15)$: [1991Din]
	$^0L_{(Al,Pt)}^{Liq} = -352540 + 114.8 * T$
	$^1L_{(Al,Pt)}^{Liq} = 68570 - 53 * T$
fcc-A1	Disordered Solution Phase: (Al,Pt)(Va)
	$^0G_{Al}^{fcc-A1}(T) - H_{Al}^{0,fcc-A1}(298.15)$: [1991Din]
	$^0G_{Pt}^{fcc-A1}(T) - H_{Pt}^{0,fcc-A1}(298.15)$: [1991Din]
	$^0L_{(Al,Pt)}^{fcc\_A1} = ULDO + DGO + 1.5 * USRO$
	$^1L_{(Al,Pt)}^{fcc\_A1} = ULD1 + DG1$
	$^2L_{(Al,Pt)}^{fcc\_A1} = ULD2 + DG2 - 1.5 * USRO$
Pt_5Al_{21}	Stoichiometric Phase: $(Al)_{0.8077}(Pt)_{0.1923}$
	$^fG_{Al:Pt}^{Pt_5Al_{21}} = 0.8077\,^0G_{Al}^{fcc-A1} + 0.1923\,^0G_{Pt}^{fcc-A1} - 56870 + 14.8 * T$
Pt_8Al_{21}	Stoichiometric Phase: $(Al)_{0.7242}(Pt)_{0.2759}$
	$^fG_{Al:Pt}^{Pt_8Al_{21}} = 0.7242\,^0G_{Al}^{fcc-A1} + 0.2759\,^0G_{Pt}^{fcc-A1} - 81805 + 23.2 * T$
$PtAl_2$	Stoichiometric Phase: $(Al)_{0.666}(Pt)_{0.334}$
	$^fG_{Al:Pt}^{PtAl_2} = 0.666\,^0G_{Al}^{fcc-A1} + 0.334\,^0G_{Pt}^{fcc-A1} - 87371 + 22.1 * T$
Pt_2Al_3	Stoichiometric Phase: $(Al)_{0.6}(Pt)_{0.4}$

	${}^{f}G_{Al:Pt}^{Pt_2Al_3} = 0.6\,{}^{0}G_{Al}^{fcc-Al} + 0.4\,{}^{0}G_{Pt}^{fcc-Al} - 89885 + 21.5*T$
PtAl	Stoichiometric Phase: $(Al)_{0.5}(Pt)_{0.5}$
	${}^{f}G_{Al:Pt}^{PtAl} = 0.5\,{}^{0}G_{Al}^{fcc-Al} + 0.5\,{}^{0}G_{Pt}^{fcc-Al} - 94071 + 24.1*T$
Beta	Stoichiometric Phase: $(Al)_{0.48}(Pt)_{0.52}$
	${}^{f}G_{Al:Pt}^{\beta} = 0.48\,{}^{0}G_{Al}^{fcc-Al} + 0.52\,{}^{0}G_{Pt}^{fcc-Al} - 92959 + 24.1*T$
Pt_5Al_3	Stoichiometric Phase: $(Al)_{0.375}(Pt)_{0.625}$
	${}^{f}G_{Al:Pt}^{Pt_5Al_3} = 0.375\,{}^{0}G_{Al}^{fcc-Al} + 0.625\,{}^{0}G_{Pt}^{fcc-Al} - 87260 + 24*T$
Pt_2Al	Stoichiometric Phase: $(Al)_{0.334}(Pt)_{0.666}$
	${}^{f}G_{Al:Pt}^{Pt_2Al} = 0.334\,{}^{0}G_{Al}^{fcc-Al} + 0.666\,{}^{0}G_{Pt}^{fcc-Al} - 85325 + 24.9*T$
$L1_2$ (Pt_3Al)	4SL-CEF: $(Al,Pt)_{0.25}(Al,Pt)_{0.25}(Al,Pt)_{0.25}(Al,Pt)_{0.25}$
	${}^{f}G_{Al:Al:Al:Pt}^{L1_2} = {}^{f}G_{Al:Al:Pt:Al}^{L1_2} = {}^{f}G_{Al:Pt:Al:Al}^{L1_2} = {}^{f}G_{Pt:Al:Al:Al}^{L1_2} = UPTAL3$
	${}^{f}G_{Al:Al:Pt:Pt}^{L1_2} = {}^{f}G_{Al:Pt:Pt:Al}^{L1_2} = {}^{f}G_{Pt:Pt:Al:Al}^{L1_2} = {}^{f}G_{Pt:Al:Al:Pt}^{L1_2} = UPTAL$
	${}^{f}G_{Al:Pt:Pt:Pt}^{L1_2} = {}^{f}G_{Pt:Al:Pt:Pt}^{L1_2} = {}^{f}G_{Pt:Pt:Al:Pt}^{L1_2} = {}^{f}G_{Pt:Pt:Pt:Al}^{L1_2} = UPT3AL$
	$L_{Al,Pt:*:*:*}^{L1_2} = L_{*:Al,Pt:*:*}^{L1_2} = L_{*:*:Al,Pt:*}^{L1_2} = L_{*:*:*:Al,Pt}^{L1_2} = UL0$
	$L_{Al,Pt:Al,Pt:*:*}^{L1_2} = L_{*:Al,Pt:Al,Pt:*}^{L1_2} = L_{*:*:Al,Pt:Al,Pt}^{L1_2} = L_{*:Al,Pt:*:Al,Pt}^{L1_2} = L_{Al,Pt:*:Al,Pt:*}^{L1_2} = USRO$
UAB	= -13595 + 8.3 * T
UPTAL	= 3 * UAB – 3913
UPTAL3	= 4 * UAB
UPT3AL	= 3 * UAB
USRO	= UAB
ULO	= 1412.8 + 5.7 * T
ULD0	= -110531 – 22.9 * T
ULD1	= -25094
ULD2	= 21475
DGO	= UPTAL3 + 1.5 * UPTAL + UPT3AL
DG1	= 2 * UPTAL3 – 2 * UPT3AL
DG2	= UPTAL3 – 1.5 * UPTAL + UPT3AL

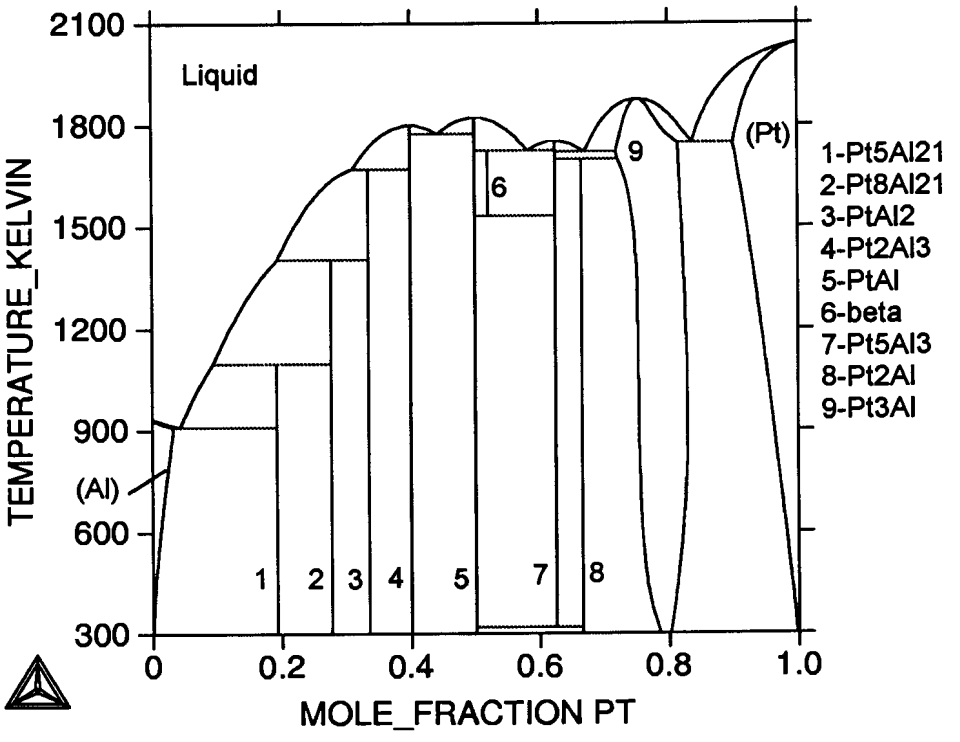

Figure 6.5. The calculated Al-Pt phase diagram.

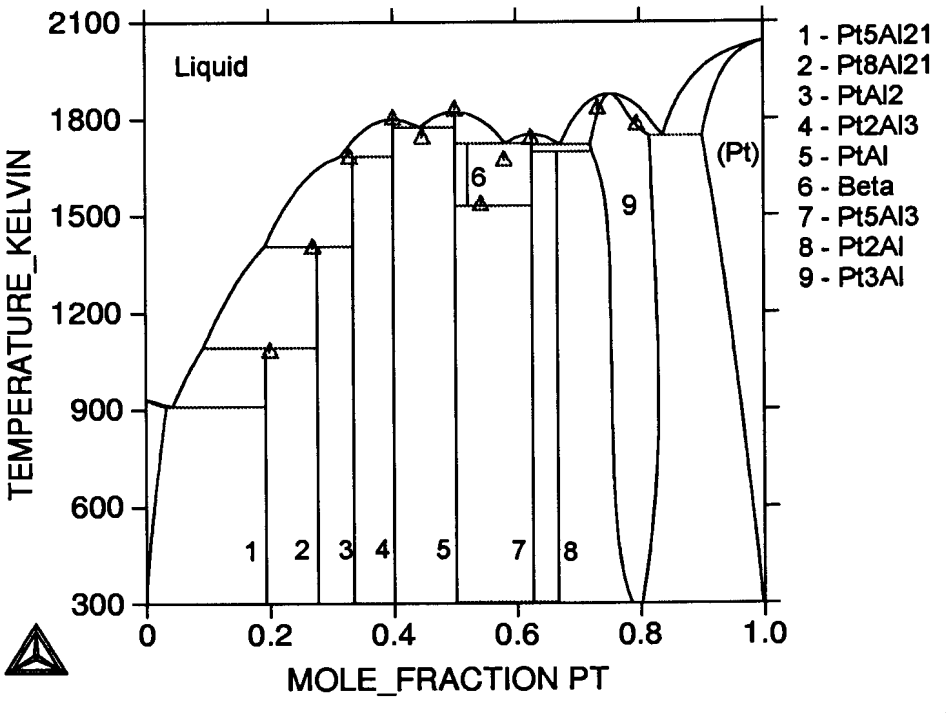

Figure 6.6. The calculated Al-Pt phase diagram compared with experimental invariant data points from the literature [1986McA].

Table 6.6. Experimental and calculated invariant temperatures and compositions for the Al-Pt system.

Reaction and Compositions (at. % Pt)					**Reaction Temperature [K]**	**Reference**
L	↔	Pt_3Al	+	(Pt)		
79.5		76.4		85.7	1780	[1986McA]
83.7		81.1		99	1748 [1]	This work
PtAl	+	L	↔	β		
50.0		53.7		51.5	1783	[1986McA]
50.0		58		52.0	1725 [2]	This work
L	↔	Pt_2Al_3	+	PtAl		
44.47		40.0		50.0	1741	[1986McA]
46.7		40.0		50	1770	This work
L	+	Pt_3Al	↔	Pt_5Al_3		
62.3		67.3		62.5	1738	[1986McA] Not included [3]
Pt_5Al_3	+	Pt_3Al	↔	Pt_2Al		
62.7		67.0		67.5	1703	[1986McA]
62.5		72		66.5	1701	This work
L	+	Pt_2Al_3	↔	$PtAl_2$		
31.8		40.0		33.3	1679	[1986McA]
40		40.0		33.3	1671	This work
L	↔	β	+	Pt_5Al_3		
55.7		57.9		66.5	1670	[1986McA]
58		52.0		62.5	1723 [4]	This work
β	↔	PtAl		Pt_5Al_3		
54.2		50.0		61.5	1533	[1986McA]
52.0		50.0		62.5	1533	This work
L	+	$PtAl_2$	↔	Pt_8Al_{21}		
18.8		32.6		27.5	1400	[1986McA]
30		33.3		27.5	1404	This work
L	+	Pt_8Al_{21}	↔	Pt_5Al_{21}		
3.1		27.5		19.2	1079	[1986McA]
9		27.5		19.2	1097	This work
L	↔	(Al)	+	Pt_5Al_{21}		
0.4		0.0		19.2	930	[1986McA]
4		3		19.2	910	This work
	L	↔	Pt_3Al			
	73.2		73.2		1829 [1]	[1986McA]
	75.3		75.3		1877	This work
	L	↔	PtAl			
	50.0		50.0		1827	[1986McA]
	50.0		50.0		1827	This work
	L	↔	Pt_2Al_3			
	40.0		40.0		1800	[1986McA]
	40.0		40.0		1800	This work
	L	↔	Pt_5Al_3			
	62.5		62.5		1800	This work [3]

[1] Pt_3Al phase at too high at. % Pt due to symmetry of 4SL CEF. See text for discussion.
[2] β phase modelled as line compound, simplification and assumed stoichiometry influences equilibria.
[3] Pt_5Al_3 in calculated diagram forms congruently and not by peritectic reaction [1986McA]. See text for discussion.
[4] 50 K too high, due to β phase model and congruent formation of Pt_5Al_3.

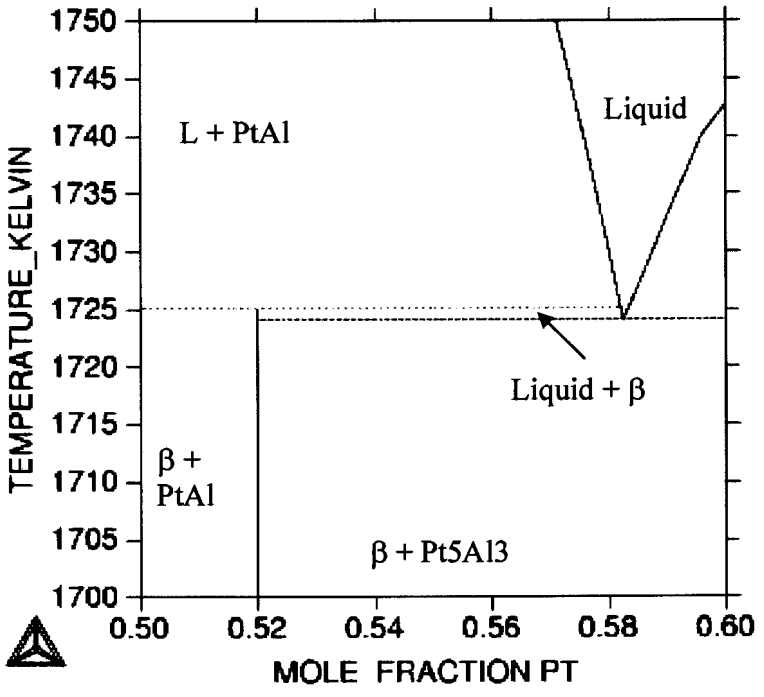

Figure 6.7. Enlargement on the Al-Pt binary system to show the reactions for the PtAl, β and liquid phases

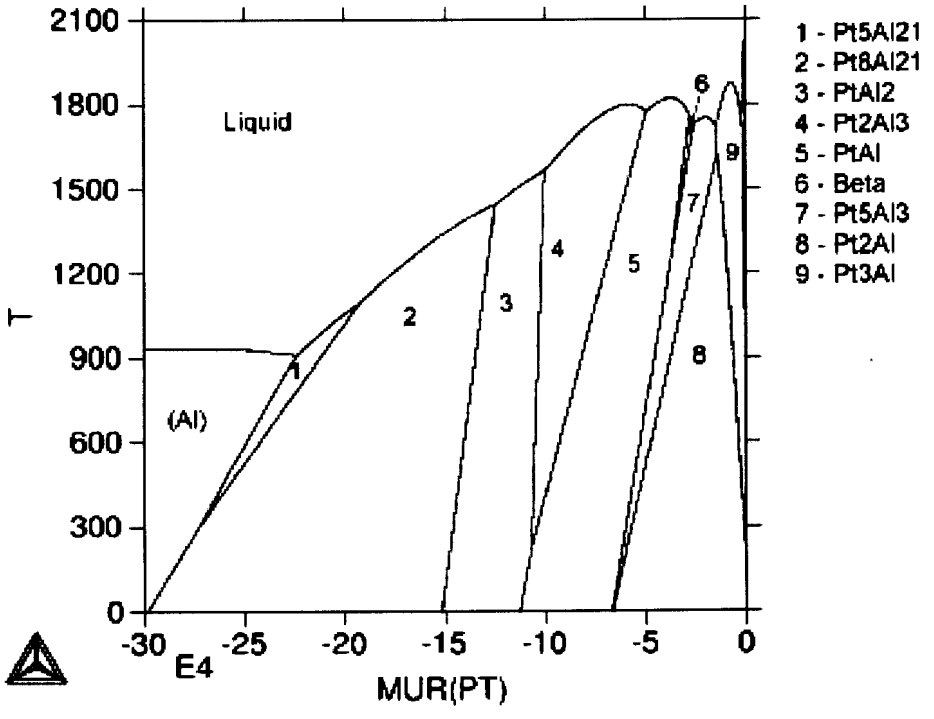

Figure 6.8The Al-Pt phase diagram of temperature against chemical potential of Pt.

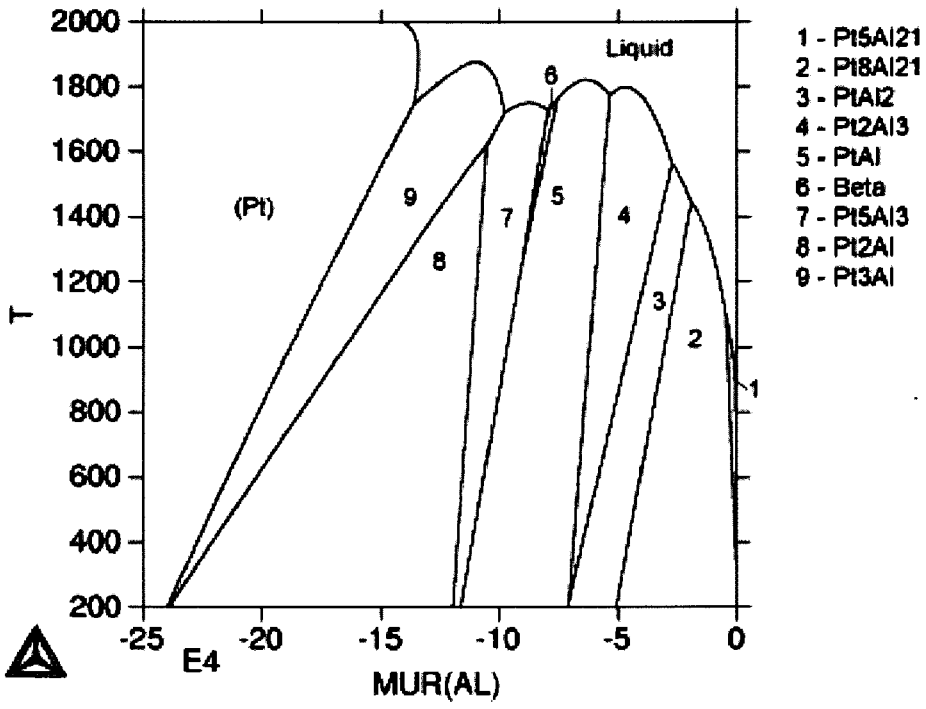

Figure 6.9. The Al-Pt phase diagram of temperature against chemical potential of Al.

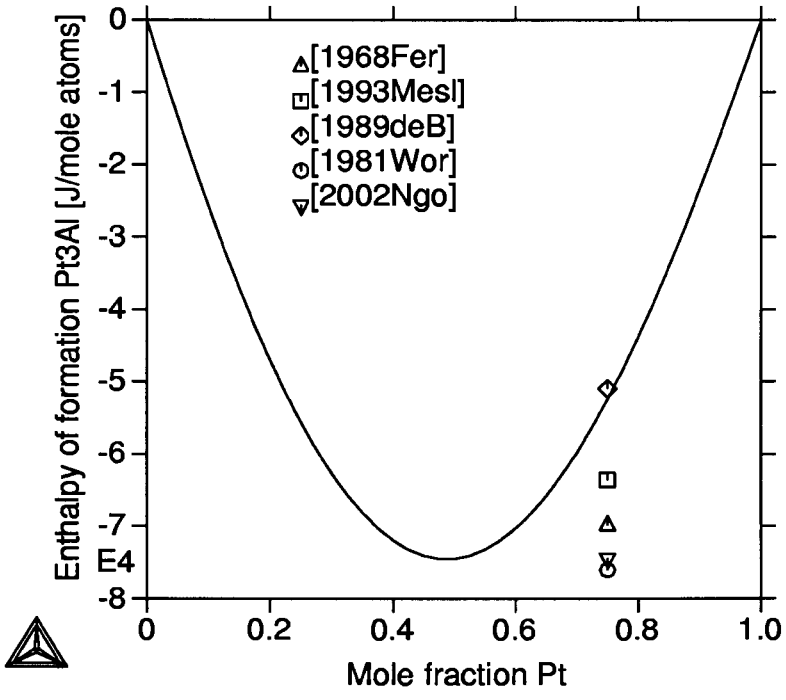

Figure 6.10. Comparison of calculated enthalpy of formation for Pt_3Al ($L1_2$) phase with experimental results [1968Fer, 1981Wor, 1993Mes], Miedema estimations [1989deB] and *ab initio* predictions [2002Ngo].

Figures 6.8 and 6.9 show the phase diagram as a function of the chemical potential instead of the composition. The slope of the curves is equal to *dG/dT,* which is the entropy of the phases. It does not show any excessive entropy contributions for any of the phases in the system, since the slopes are all more or less similar. The decomposition of the β phase (phase number 6) is shown, as well as the solid-state formation of the Pt_2Al phase (phase number 8).

Table 6.7. Experimental and calculated enthalpies of formation for the Al-Pt system.

Phase	ΔH_f [J/mole atoms]	**Method**	**Reference**
Pt_5Al_{21}	-57 320	Solute solvent drop calorimetry	[1968Fer]
	-56 827	Calculated	This work
Pt_8Al_{21}	-71 130	Solute solvent drop calorimetry	[1968Fer]
	-81 751	Calculated	This work
$Pt\ Al_2$	-84 000	Solute solvent drop calorimetry	[1968Fer]
	-87 325	Calculated	This work
Pt_2Al_3	-94 980	Solute solvent drop calorimetry	[1968Fer]
	-79 000	Miedema semi-empirical method	[1988deB]
	-96 500	Direct Synthesis Calorimetry	[1993Mes]
	-89 839	Calculated	This work
PtAl	-100 420	Solute solvent drop calorimetry	[1968Fer]
	-100 000	Direct Synthesis Calorimetry	[1991Jun]
	-82 000	Miedema semi-empirical method	[1988deB]
	-67 440	*Ab initio*	[2002Ngo]
	-94 025	Calculated	This work
β	-91 300	Calorimetry*	[1968Fer]
	-92 913	Calculated	This work
Pt_5Al_3	-90 730	Miedema semi-empirical method	[1988deB
	-87 213	Calculated	This work
Pt_2Al	-88 280	Miedema semi-empirical method	[1988deB
	-85 278	Calculated	This work
Pt_3Al	-69 870	Solution Calorimetry	[1968Fer]
	-63 600	Direct Synthesis Calorimetry	[1993Mes]
	-50 990	Miedema semi-empirical method	[1988deB]
	-76 000**	Electrochemical	[1981Wor]
	-74 380	*Ab initio*	[2002Ngo]
	-51 668	Calculated	This work

* estimated from the curve fitted to the enthalpies of formation experimentally determined by Ferro *et. al.* [1968Fer].
** estimated from the Gibbs free energy of mixing ΔGm = -76 640 + 7.48*T [1981Wor].

The calculated enthalpies of formation are compared to the experimental values in Table 6.7. They are all within the 10% error of Ferro's [1968Fer] experimental results, except for Pt_3Al, which is much lower, indicating the predicted phase is more stable than the experimental phase. This can also be affected by the fact the Pt_3Al forms at 73.2 at. % Pt

and not the expected stoichiometric 75 at % Pt of the perfect crystal structure, and the modelling could not fit the composition to 73.2 at. % Pt for the congruent melting. The enthalpy of formation for the Pt_3Al phase is compared with the experimental and *ab initio* predicted values in Figure 6.10.

Although there are some differences between the calculated and experimental Al-Pt phase diagrams, these are in areas where limited experimental data are available. In some cases the experimental diagram is based on the results on only one report. The limited data forced the need for simplified models, especially for the β phase. Thus the data appear to be not in good agreement, however, it is due to the simplified model. Considering the assumptions and limited data, the calculated phase diagram is in general excellent agreement with the experimental phase diagram.

6.4.3 Al-Pt-Ru

The predicted liquidus surface projection is shown in Figures 6.10 and 6.11. The solidification reactions are listed in Table 6.9. The reaction types were identified by projecting the surface on a temperature against liquid composition diagram (Figure 6.12). Ternary eutectic reactions were recognised by the meeting of three lines, forming a local minimum. A true ternary peritectic was identified by one of the line above the reaction, and two below [1965Wes].

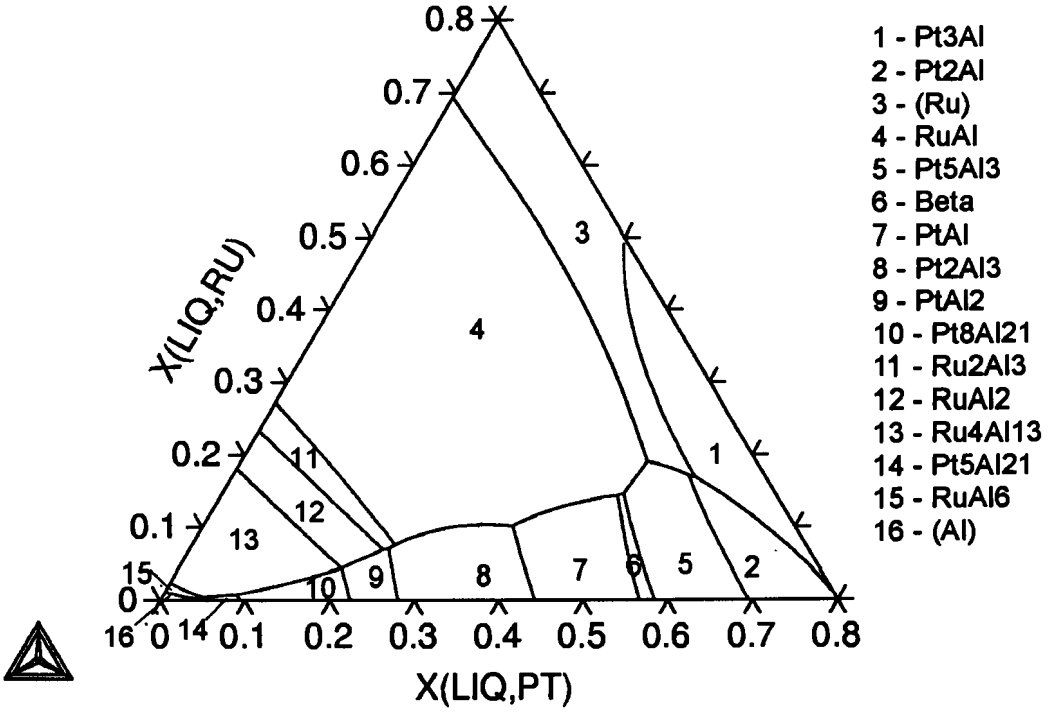

Figure 6.11. Liquidus surface projection for Al-Pt-Ru, indicating liquidus surface areas for the phases.

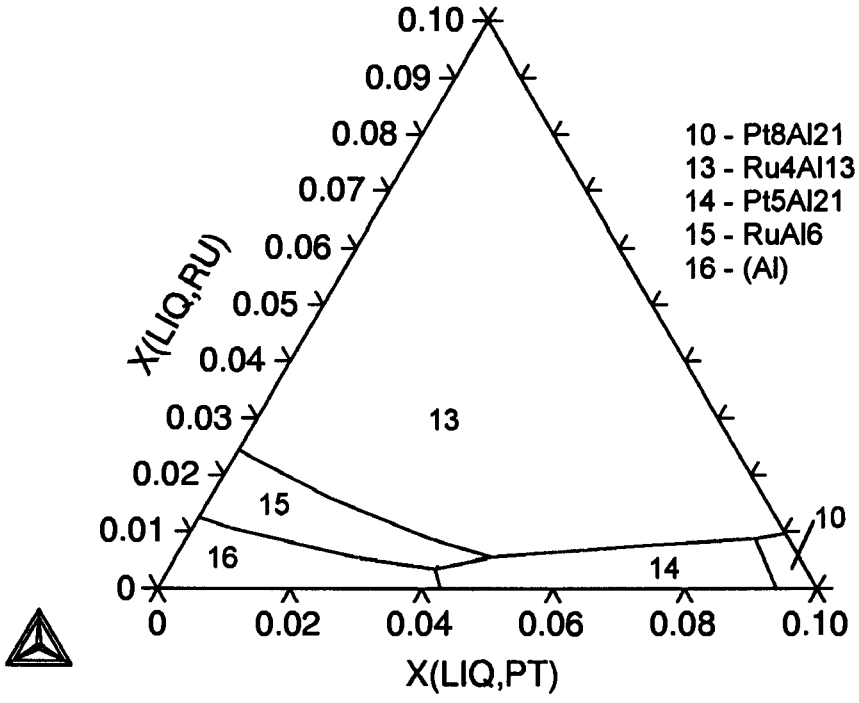

Figure 6.12. Enlargement of the Al-corner of the Al-Pt-Ru liquidus projection (Figure 6.10).

The solidification projection is only presented up to 80 at. % Pt. Although the Thermo-Calc software calculated individual equilibrium values above this composition, it was not possible to map the liquidus projection for the area above 80 at. %. This is probably due to the 4SL CEF description of the Pt_3Al phase, as this phase is too stable in this projection, giving a too large phase surface on the liquidus projection. The extrapolation gives about 10 at% Ru in Pt_3Al, while experimental work [2001Big1, 2001Big2, 2001Hil1] showed a limited solubility of ruthenium in Pt_3Al. No attempts have been made to correct this at this stage. No thermodynamic data are yet available for the Al-Pt-Ru system, and an optimisation without thermodynamic data to give the liquid a reference point, would be meaningless.

Very little has been published to date on ternary extrapolations and ternary optimisations using the 4SL-CEF. Kuskoffsky [2002Kus1, 2002Kus2] evaluated the use of ternary parameters in the 4SL-CEF, and calculated the Ag-Au-Cu ternary. It was noted that care had to be taken with the reciprocal parameters. In the case of Ag-Au-Cu, data on the bonding energies of nearest neighbours and next-nearest neighbours were available to allow successful use of the 4SL-CEF.

Reactions 1 and 2 in Table 6.8 include the formation of Pt_2Al. This is an artefact of the modelling, again probably due to the use of 4SL-CEF. In the binary, Pt_2Al forms by a solid-state eutectoid reaction, $Pt_5Al_3 + Pt_3Al \rightarrow Pt_2Al$. Pt_2Al should, therefore, not form

from the liquid as it does in this extrapolation. However, it is possible that the presence of a third element in a binary structure can change the reaction in the ternary. In this case the extrapolation stabilised the Pt_2Al phase too much.

Table 6.8. Solidification sequence for Al-Pt-Ru.

Equation number	Reaction	Temperature [K]
1	$L + Pt_3Al \rightarrow (Ru) + Pt_2Al$	1445
2	$L \rightarrow (Ru) + Pt_5Al_3 + Pt_2Al$	1443
3	$L \rightarrow RuAl + Pt_5Al_3 + (Ru)$	1435
4	$L + \beta \rightarrow RuAl + Pt_5Al_3$	1485
5	$L + PtAl \rightarrow RuAl + \beta$	1500
6	$L \rightarrow RuAl + Pt_2Al_3 + PtAl$	1620
7	$L + RuAl \rightarrow Ru_2Al_3 + Pt_2Al_3$	1525
8	$L + Pt_2Al_3 \rightarrow Ru_2Al_3 + PtAl_2$	1507
9	$L + Ru_2Al_3 \rightarrow RuAl_2 + PtAl_2$	1500
10	$L + PtAl_2 \rightarrow Ru_4Al_{13} + Pt_8Al_{21}$	1415
11	$L + RuAl_2 \rightarrow Ru_4Al_{13} + Pt_8Al_{21}$	1408
12	$L + Pt_8Al_{21} \rightarrow Ru_4Al_{13} + Pt_5Al_{21}$	1080
13	$L + Ru_4Al_{13} \rightarrow RuAl_6 + Pt_5Al_{21}$	945
14	$L \rightarrow (Al) + RuAl_6 + Pt_5Al_{21}$	900

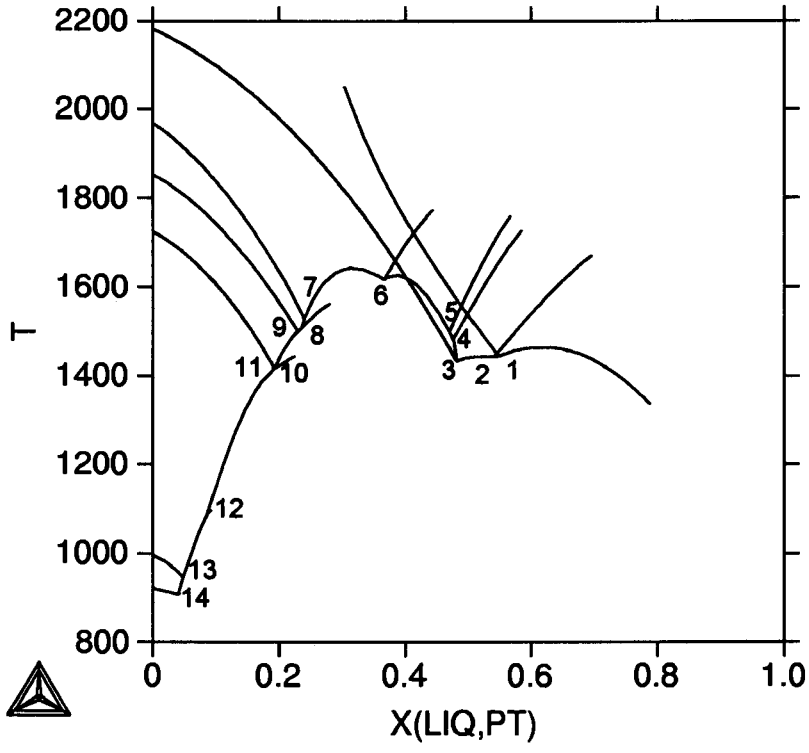

Figure 6.13. Projection of temperature against composition to identify the reaction types.

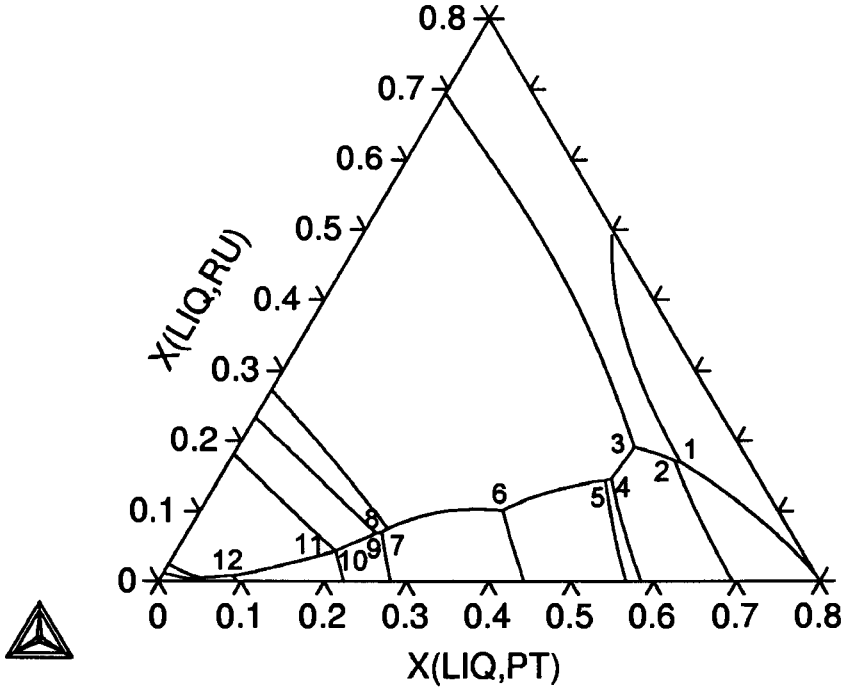

Figure 6.14. Solidification reactions, as listed in Table 6.8.

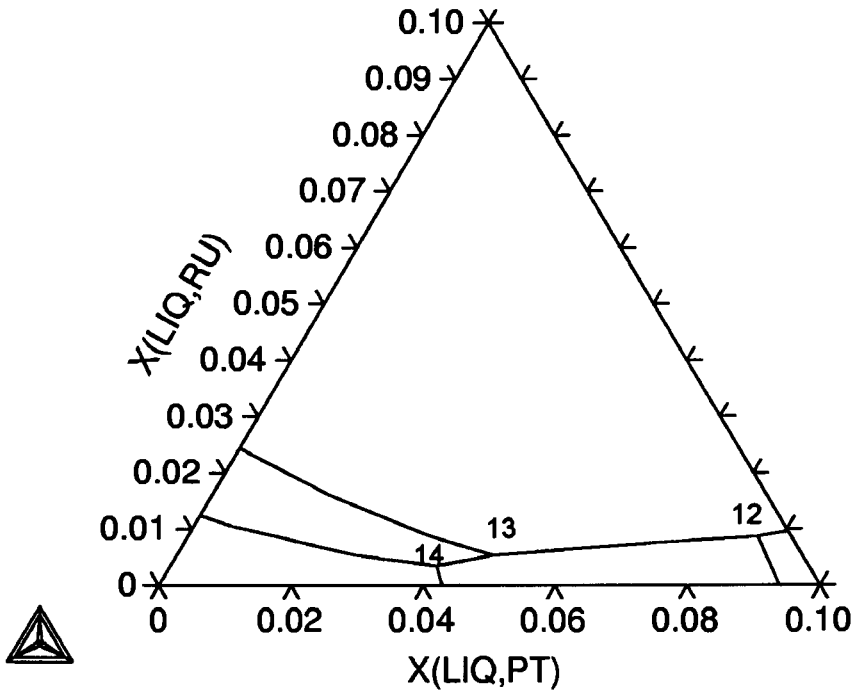

Figure 6.15. Solidification reactions, as listed in Table 6.8 (enlargement of Al-corner in Figure 6.13)

6.5 Conclusions

Stable Gibbs energy functions have been calculated for the phases in the Al-Ru and Al-Pt phase diagrams. Two models have been used to describe the ordered RuAl-B2 phase in the Al-Ru system. The results from MSL model were in better agreement with results from the literature. Although there were some areas of lesser agreement in the calculated Al-Pt system, they can be contributed to the 4SL CEF that has been used, as well as a lack on experimental data for the β-phase, which necessitated the stoichiometric treatment of the phase.

The ternary Al-Pt-Ru phase diagram was extrapolated from the calculated binary phase diagrams. The extrapolated diagram is in good agreement with the experimental diagram. The major differences arised from the fact that two new ternary phases were found in the experimental study. Since an extrapolation was based on the Gibbs energy functions for already entered phases, the software could not predict these new phases.

The good agreement between the experimental and calculated liquidus surface projections proves that thermodynamic modeling is powerful technique in the development of new alloy systems.

Chapter 7
Comparison of Experimental and Computational Results

7.1 Introduction

The results of the experimental determined Al-Pt-Ru liquidus surface projection and solidification reaction scheme are compared to the predicted liquidus projection and solidification reaction sequence. The agreements and discrepancies are discussed.

7.2 Results and discussion

Figures 7.1 and 7.2 show the experimental and predicted liquidus surface projections respectively. The results are in good agreement except for the Pt_3Al liquid surfaces, which is more stable in the predicted diagram than in the experimental diagram. The predicted phase diagram does not include the two ternary phases, X and T, which were found in the experimental investigation.

The solidification reactions are compared in Tables 7.1 and 7.2. There are some inconsistencies when comparing the experimentally deduced solidification sequence and the sequence predicted from the calculated Al-Pt-Ru system.

In the experimental solidification sequence, not enough data were available to determine the solidification direction of some of the reactions (direction of liquidus slope) listed in Table 7.1. However for most reactions the direction of decreasing temperature could be deduced. For the reaction at E, the data were not enough to decide which reaction is more probable. Both possible reactions are listed.

In the predicted system, the ~Pt_3Al phase area is too large, implying the calculated Gibbs energy function is too stable relative to the function for the (Pt). The predicted solidification reactions 1 and 2 in Table 7.2 show the Pt_2Al phase forming from a liquid reaction. In the Al-Pt binary system, Pt_2Al forms from the solid state through a peritectoid reaction. Although it is possible that the presence of a third element in a binary phase can change the behaviour of the phase, e.g. stabilise it to higher temperatures, the results from the extrapolation is not in agreement with the experimental results. The experimental results did not show Pt_2Al forming during solidification.

Reactions C and D from the experimental solidification sequence compare with reactions 3 and 4 in the predicted solidification sequence, although the reaction types differ. This could be either due to not enough experimental data or due to the extrapolation from pure binary phases without taking into account the possible effect of a third element on the Gibbs energy functions of the binary phases.

The ternary extrapolation also does not include the two ternary phases, as the extrapolation is based on phases already entered in the data file. Thus the rest of the solidification sequence cannot be compared beyond reactions 4 and D.

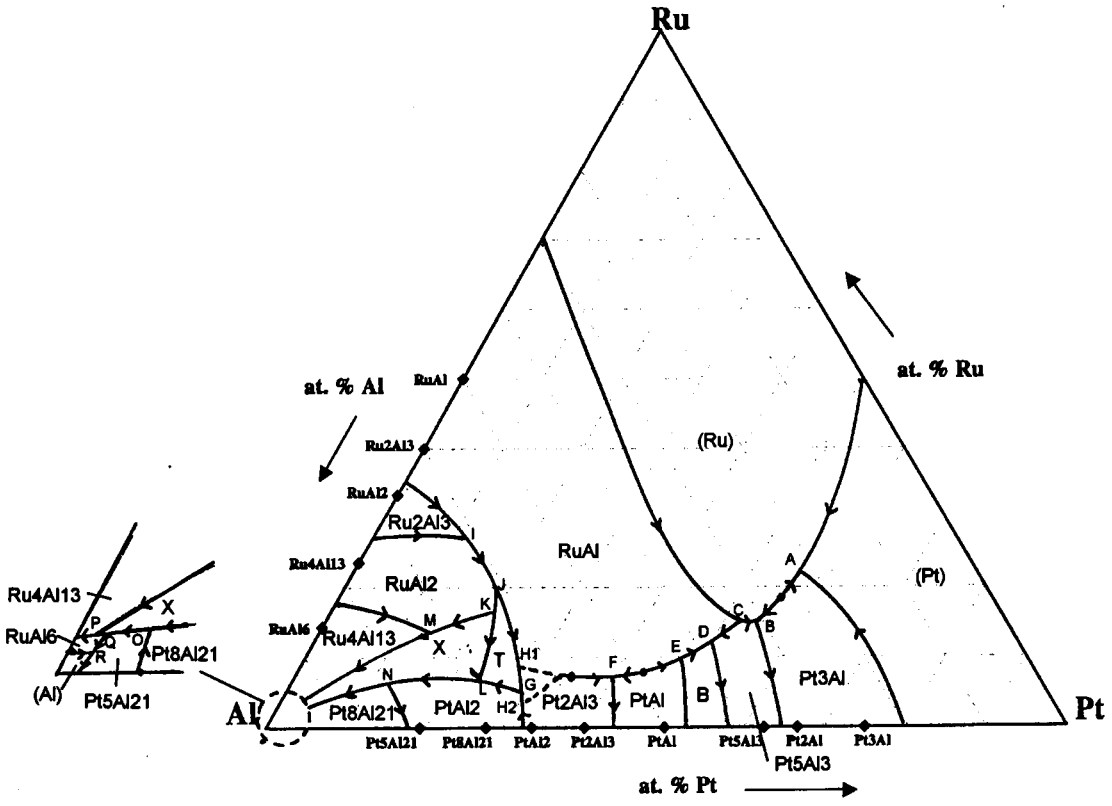

Figure 7.1. Experimental liquidus surface projection, showing the solidification reactions (A-R).

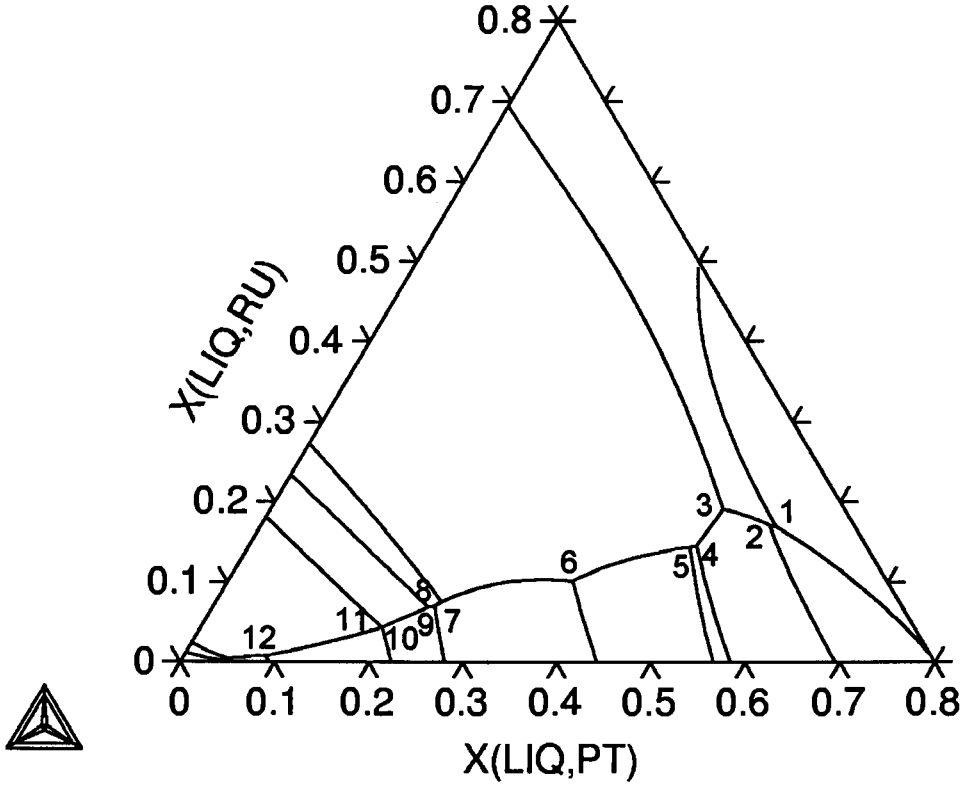

Figure 7.2. Predicted liquidus surface projection, showing the solidification reactions (1-12).

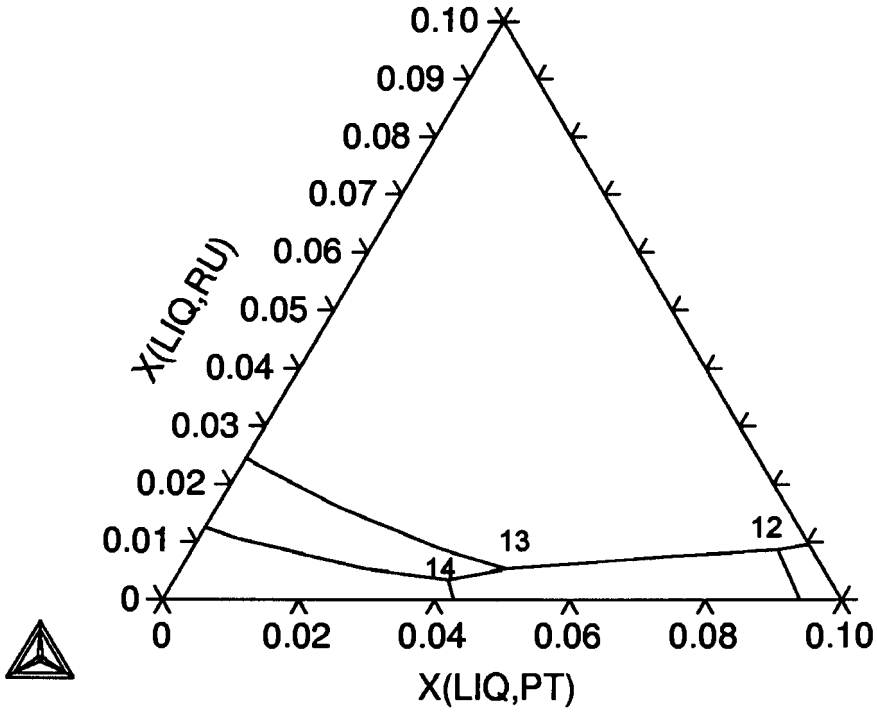

Figure 7.3 Predicted liquidus surface projection for the Al-corner, showing the solidification reactions (1-12) (enlargement of the Al-corner from Figure 7.2).

7.3 Conclusions

Although there are some discrepancies, the general comparison is excellent. The comparison of the experimentally determined and calculated prediction shows that predicting phase diagrams through computational methods is a useful tool for the metallurgist. The discrepancies in the comparison are mainly due to the absence of the two new ternary phases in the extrapolated phase diagram. To include these the ternary lattice stabilities will have to be calculated through an optimisation procedure, which fell outside the scope of this study.

In the continuation of the project, which this study was part of, this predicted ternary phase diagram will be used to select experimental points for further investigation in order to obtain maximum results from them.

Table 7.1. Experimental solidification reactions for Al-Pt-Ru (indicated in Figure 7.1).

Equation number	Reaction
A	$L \rightarrow (Ru) + (Pt) + \sim Pt_3Al$
B	$L + (Ru) \rightarrow Pt_5Al_3 + \sim Pt_3Al$
C	$L + (Ru) + \sim RuAl \rightarrow \sim Pt_5Al_3$
D	$L + \sim RuAl \rightarrow \beta + \sim Pt_5Al_3$
E *	($\uparrow$) $L + \sim PtAl \rightarrow \sim RuAl + \beta$ ($\downarrow$) $L + \sim PtAl + \sim RuAl \rightarrow \beta$
F	$L + \sim RuAl \rightarrow \sim PtAl + Pt_2Al_3$
G* H1*	$L + Pt_2Al_3 \rightarrow \sim PtAl_2 + \sim Ru_{18}Pt_{28}Al_{64}$ $L + \sim RuAl \rightarrow \sim Ru_{18}Pt_{28}Al_{64} + Pt_2Al_3$
G* H2*	$L + \sim RuAl \rightarrow \sim PtAl_2 + \sim Ru_{18}Pt_{28}Al_{64}$ $L + Pt_2Al_3 \rightarrow \sim RuAl + \sim PtAl_2$
I	$L + Ru_2Al_3 \rightarrow \sim RuAl + \sim RuAl_2$
J	$L + \sim RuAl + \sim RuAl_2 \rightarrow \sim Ru_{18}Pt_{28}Al_{64}$
K	$L + \sim Ru_{18}Pt_{28}Al_{64} + \sim RuAl_2 \rightarrow \sim Ru_{12}Pt_{15}Al_{73}$
L	$L + \sim Ru_{18}Pt_{28}Al_{64} \rightarrow \sim Ru_{12}Pt_{15}Al_{73} + \sim PtAl_2$
M	$L + \sim RuAl_2 \rightarrow \sim Ru_{12}Pt_{15}Al_{73} + \sim Ru_4Al_{13}$
N	$L + \sim PtAl_2 + \sim Ru_{12}Pt_{15}Al_{73} \rightarrow \sim Pt_8Al_{21}$
O	$L + \sim Pt_8Al_{21} \rightarrow \sim Ru_{12}Pt_{15}Al_{73} + \sim Pt_5Al_{21}$
Q	$L + \sim Ru_{12}Pt_{15}Al_{73} + \sim Pt_5Al_{21} \rightarrow \sim RuAl_6$
P**	$L + \sim Ru_{12}Pt_{15}Al_{73} \rightarrow \sim Ru_4Al_{13} + \sim RuAl_6$
R	$L + \sim RuAl_6 \rightarrow \sim Pt_5Al_{21} + (Al)$

* Not enough experimental data available to conclude in which direction this reaction proceeds.
** Exit reaction must be peritectic to be consistent with the Al-Ru binary.

Table 7.2. Predicted solidification reactions for the calculated Al-Pt-Ru system.

Equation number	Reaction
1	$L + Pt_3Al \rightarrow (Ru) + Pt_2Al$
2	$L \rightarrow (Ru) + Pt_5Al_3 + Pt_2Al$
3	$L \rightarrow RuAl + Pt_5Al_3 + (Ru)$
4	$L + \beta \rightarrow RuAl + Pt_5Al_3$
5	$L + PtAl \rightarrow RuAl + \beta$
6	$L \rightarrow RuAl + Pt_2Al_3 + PtAl$
7	$L + RuAl \rightarrow Ru_2Al_3 + Pt_2Al_3$
8	$L + Pt_2Al_3 \rightarrow Ru_2Al_3 + PtAl_2$
9	$L + Ru_2Al_3 \rightarrow RuAl_2 + PtAl_2$
10	$L + PtAl_2 \rightarrow Ru_4Al_{13} + Pt_8Al_{21}$
11	$L + RuAl_2 \rightarrow Ru_4Al_{13} + Pt_8Al_{21}$
12	$L + Pt_8Al_{21} \rightarrow Ru_4Al_{13} + Pt_5Al_{21}$
13	$L + Ru_4Al_{13} \rightarrow RuAl_6 + Pt_5Al_{21}$
14	$L \rightarrow (Al) + RuAl_6 + Pt_5Al_{21}$

Conclusions and recommendations

Conclusions

The Al-Pt-Ru phase diagram was investigated experimentally and a liquidus surface projection is proposed. The experimental results were compared to a predicted liquidus surface projection using the CALPHAD method.

The following conclusions may be drawn from the experimental results:

- The liquidus surface is dominated by the RuAl phase; it occurred to within 10 at. % of the Al-Pt binary.
- (Ru) also has a large liquidus surface. This is an important factor to consider when making alloys that are just outside of the region of the alloys targeted for commercialisation.
- RuAl was found to contain at least 20 at. % platinum
- $PtAl_2$ exhibited up to 11 at. % solubility for ruthenium.
- $RuAl_2$ exhibited up to 10 at. % solubility for platinum.
- Ru_4Al_{13} and $RuAl_6$ were difficult to analyse, since they were found together on a fine scale.
- $RuAl_6$ showed solubility of at least 10 at. % platinum.
- Most of the other phases showed limited solubilities for the ternary element, less than 2 at. %: Ru_4Al_{13}, Pt_2Al_3, Pt_5Al_3, Pt_5Al_{21} and PtAl.
- A ternary phase X, with a composition ~$Ru_{12}Pt_{15}Al_{73}$, was found to be present. Initial XRD analysis showed that the X phase probably has a primitive cubic structure and is similar to ~$RhAl_{2.63}$ and ~$IrAl_{2.75}$ .The lattice parameter is 0.7712 nm.
- A high-temperature ternary phase T, with composition of ~$Ru_{18}Pt_{28}Al_{64}$, exists.
- Ru_2Al_3, T and β decomposed through solid-state reactions:
  $Ru_2Al_3 \rightarrow$ ~RuAl + ~$RuAl_2$
  T $\rightarrow$ X + ~$PtAl_2$
  β $\rightarrow$ ~PtAl + Pt_5Al_3
- ~RuAl was involved in a number of subsequent reactions in different alloys:
  - peritectic formation of ~PtAl,
  - peritectic formation of ~$PtAl_2$
  - peritectic formation of β phase of the Al-Pt binary.
- There was good agreement between the experimental EDS and XRD results, despite the lack of data on some of the phases present in the ICDD. In many cases, the

structures of prototypes could be used through a grain refinement process to identify the binary phases.

The binary phase diagrams were calculated with the Thermo-Calc software, using the CALPHAD method. The calculated binaries are in excellent agreement with the experimentally reported phase diagrams in the literature. Furthermore, a liquidus surface projection has also been predicted from extrapolating the ternary system from the calculated binaries. The predicted results are in good agreement with the experimental results, thus showing that computational thermodynamics is a powerful tool in alloy development. Thermo-Calc did not provide any evidence for the ternary phases, which is not surprising.

Recommendations:

- Thermal analysis should be conducted on some of the samples to obtain reaction temperature and thermodynamic values (enthalpy of formation) for phases in the system, as these are required for the further optimisation of the ternary system. DTA, DSC, TG and calorimetry should be considered.
- Samples should be heat treated, as this will bring them to equilibrium conditions. This would assist in the XRD analyses (some heat treatments were done at 600°C, although 1000°C would be more relevant for the future applications of Pt-based alloys. Analysis of the samples after heat treatments is in progress and is part of a continuing project.).
- *Ab initio* predictions could be useful in predicting the enthalpies of formation for some of the binary phases, and the new ternary phases. More ab initio calculations on the polymorphs of the $L1_2$ phase would be valuable information for the CALPHAD modeling of this part of the Al-Pt phase diagram.
- XRD work should be conducted on especially the binary Al-Pt system, as very little standard data is available (this is planned as part of the current continuing project).
- TEM studies of samples containing the ternary phases would be needed to confirm the crystal structures.
- The calculated ternary phase diagram should be optimised. The ternary phases must be included. However, this is subject to first obtaining some thermodynamic values of the phases and suggesting crystal structure models for the new ternary phases. The optimisation will also solve the current discrepancies in phase stabilities with the experimental results.
- Re-optimisation of the Al-Pt system. A change in the use of the 4 SL CEF has been proposed after this work was submitted. The metastable phase diagram for the fcc ordered and disordered phases must first be optimised using *ab initio* calculated enthalpies of formation. Once an acceptable description for the fcc phases has been obtained, the complete system should be optimised in such a way that the metastable phases are not stable in the optimised system. The revised optimisation and use of the model will be published in the CALPHAD journal.